



Hamburg University of Applied Sciences

Faculty of Life Sciences

**Mitigation of the potential induced degradation of photovoltaic modules and its impact on  
the performance of solar parks**

Master Thesis

Renewable Energy Systems – Environmental and Process Engineering Master

submitted by

Jan Vollers



Hamburg

on 11. March 2022

Reviewer: Prof. Dr. Frerk Haase (HAW Hamburg)

Reviewer: M.Sc. Michael Falkenberg (CEE Operations GmbH)

in cooperation with the company: CEE Operations GmbH

## I. Abstract

This master thesis gives an overview of the impact of the potential induced degradation (PID) effect in a portfolio of several multi-megawatt ground-mounted solar parks and how this effect can be prevented and reversed. The so-called photovoltaics power booster (PVPB) box is used, which applies a repair voltage to the array of photovoltaic modules at night and thus reverses the PID effect. One central inverter station is equipped with a PVPB box for each solar park. Its specific yield values are then put into proportion with the specific yield values of the remaining inverter stations representing the reference area. Technical failures of yield-relevant equipment and days with snowfall are considered and excluded from the evaluation. The results are mixed and show partly positive developments on the yield and partly no development. Most of the PVPB boxes have only been in operation for two to three months during the winter, which is weak in irradiation and makes the evaluation less accurate. The evaluation phase should be extended until at least some months with suitable irradiation are included in the analysis and therefore be repeated in May or June. However, it can be said that the PID effect will remain an existing problem in the future, as the modules will not be built PID-free, and the costs for module production must be kept as low as possible. Furthermore, modules can be labeled as PID-free according to the TS IEC 62804-1:2015-08 standard if they have power losses due to PID of less than 5%. The effect will probably even increase since the maximum system voltage of new solar parks is up to 1500 V instead of the previous 1000 V.

## II. Table of Content

<b>I. Abstract</b> .....	<b>I</b>
<b>II. Table of Content</b> .....	<b>II</b>
<b>III. List of Figures</b> .....	<b>IV</b>
<b>IV. List of Tables</b> .....	<b>VII</b>
<b>V. List of Abbreviation</b> .....	<b>VIII</b>
<b>1. Introduction</b> .....	<b>1</b>
<b>2. Fundamentals</b> .....	<b>3</b>
2.1 Photoelectric Effect.....	3
2.2 Electrical Description of Real Solar Cells .....	4
2.3 Structure of a Solar Cell .....	6
2.4 Structure of a Photovoltaic Module .....	7
2.5 Structure of a Solar Park.....	9
2.6 Potential Induced Degradation .....	11
2.7 Detection of the PID Effect .....	13
2.8 Prevention and Inversion of the PID-effect.....	16
<b>3. Materials and Methods</b> .....	<b>19</b>
3.1 Market Overview.....	19
3.2 Location of Installation .....	22
3.3 Selection of Reference Inverter .....	24
3.4 Overview of the Portfolio .....	24
3.4.1 EHEU – Solar Park Bavaria North .....	25
3.4.2 FOR – Solar Park Brandenburg East .....	27
3.4.3 HAI – Solar Park Bayreuth.....	29
3.4.4 RICH – Solar Park Miltenberg .....	31
3.4.5 KAL – Solar Park Saxony-Anhalt North.....	33
3.4.6 HAL – Solar Park Saxony-Anhalt West .....	34
3.4.7 FREI – Solar Park Mannheim .....	35
3.4.8 EGG – Solar Park Berlin East .....	37
3.4.9 AHL – Solar Park Bremen .....	39
3.4.10 ROHR – Solar Park Thuringia South.....	42
3.4.11 ELS – Solar Park Saxony East.....	44
3.5 Cost Breakdown .....	46

Table of content

---

3.6	Analysis Method.....	48
3.7	Dedicated Voltage Measurement in AHL .....	49
<b>4.</b>	<b>Results.....</b>	<b>52</b>
4.1	Yield Gain .....	52
4.2	Field Measurements .....	58
4.3	Commercial Evaluation .....	62
<b>5.</b>	<b>Discussion.....</b>	<b>67</b>
5.1	Evaluation of Results.....	67
5.2	Possible Errors .....	67
5.3	Influence of the Season .....	69
5.4	Personal Safety Risk .....	69
5.5	Risk Analysis.....	71
5.6	Outlook & Recommendation .....	72
<b>6.</b>	<b>Summary .....</b>	<b>74</b>
<b>VI.</b>	<b>References.....</b>	<b>IX</b>
<b>VII.</b>	<b>Affidavit.....</b>	<b>XIV</b>
<b>VIII.</b>	<b>Appendix .....</b>	<b>XV</b>

### III. List of Figures

Figure 2-1 bandgap diagram.....	3
Figure 2-2 Single-diode model of a solar cell .....	4
Figure 2-3 Influence of series resistance $R_S$ on the solar cell characteristic curve.....	5
Figure 2-4 Influence of shunt resistance $R_{Sh}$ on the solar cell characteristic curve.....	5
Figure 2-5 Structure of a solar cell .....	6
Figure 2-6 space charge region at the p-n junction .....	6
Figure 2-7 Schematic structure of a photovoltaic module .....	7
Figure 2-8 Structural components of a photovoltaic module .....	8
Figure 2-9 Concept of central inverters .....	9
Figure 2-10 Concept of string inverter .....	10
Figure 2-11 Exemplary depiction of a string voltage .....	12
Figure 2-12 Generator potential example for an MPP voltage of 400V.....	13
Figure 2-13 EL image of a PID affected module (left) and I-V characteristic of individual cells .....	13
Figure 2-14 string IV-curve measurements of an example solar energy system which is affected by PID .....	14
Figure 2-15 EL image of a floating PID string with degraded panels on the side with negative potential.....	14
Figure 2-16 electroluminescence (left) and thermographic (right) image of a with PID affected module .....	15
Figure 2-17 Q.Plus L-G4.2 Anti-PID Feature .....	15
Figure 2-18 Voltage divider model for PID on module level .....	16
Figure 2-19 Measurement of the voltage across $SiN_x$ layer .....	17
Figure 3-1 float controller day mode .....	20
Figure 3-2 float controller night mode .....	20
Figure 3-3 PVPB SI 30-3.....	21
Figure 3-4 PVPB Extender .....	22
Figure 3-5 basic connection design of a PVPB.....	23
Figure 3-6 Connection of PVPB to DC busbar.....	24
Figure 3-7 Solar Park EHEU satellite picture.....	26

## List of Figures

---

Figure 3-8 schematics of the PVPB installation in the solar park EHEU .....	27
Figure 3-9 Solar Park FOR satellite picture .....	28
Figure 3-10 schematics of the PVPB installation in the solar park FOR .....	29
Figure 3-11 Solar Park HAI satellite picture.....	30
Figure 3-12 schematics of the PVPB installation in the solar park HAI .....	31
Figure 3-13 Solar Park RICH satellite picture .....	32
Figure 3-14 schematics of the PVPB installation in the solar park RICH .....	33
Figure 3-15 Solar Park HAL satellite picture .....	34
Figure 3-16 schematics of the PVPB installation in the solar park HAL.....	35
Figure 3-17 Solar Park FREI satellite picture.....	36
Figure 3-18 schematics of the PVPB installation in the solar park FREI .....	37
Figure 3-19 Solar Park EGG satellite picture.....	38
Figure 3-20 schematics of the PVPB installation in the solar park EGG .....	39
Figure 3-21 Solar Park AHL satellite picture .....	39
Figure 3-22 schematics of the PVPB installation in the solar park AHL1-2 .....	41
Figure 3-23 schematics of the PVPB installation in the solar park AHL3-5 .....	42
Figure 3-24 Solar Park Thuringia South satellite picture .....	42
Figure 3-25 schematics of the PVPB installation in the solar park ROHR.....	44
Figure 3-26 Solar Park ELS satellite picture .....	44
Figure 3-27 schematics of the PVPB installation in the solar park ELS.....	46
Figure 3-28 Installation of the dedicated voltage measurement .....	50
Figure 4-1 EHEU results (right: period with PVPB installed; left: same period one year earlier) .....	52
Figure 4-2 FOR results (right: period with PVPB installed; left: same period one year earlier) .....	52
Figure 4-3 HAI results (right: period with PVPB installed; left: same period one year earlier)	53
Figure 4-4 RICH results (right: period with PVPB installed; left: same period one year earlier) .....	53
Figure 4-5 HAL results (right: period with PVPB installed; left: same period one year earlier) .....	54
Figure 4-6 FREI results (right: period with PVPB installed; left: same period one year earlier) .....	54

## List of Figures

---

Figure 4-7 EGG results (right: period with PVPB installed; left: same period one year earlier) .....	54
Figure 4-8 AHL1 results (right: period with PVPB installed; left: same period one year earlier) .....	55
Figure 4-9 AHL2 results (right: period with PVPB installed; left: same period one year earlier) .....	55
Figure 4-10 AHL3 results (right: period with PVPB installed; left: same period one year earlier) .....	56
Figure 4-11 AHL4 results (right: period with PVPB installed; left: same period one year earlier) .....	56
Figure 4-12 AHL5 results (right: period with PVPB installed; left: same period one year earlier) .....	57
Figure 4-13 ROHR results (period with PVPB installed) .....	57
Figure 4-14 ELS results (right: period with PVPB installed; left: same period one year earlier) .....	57
Figure 4-15 Voltage Measurement from 10.11.2021 12:00 until 11.11.2021 11:59 .....	60
Figure 4-16 Voltage measurement in AHL $V_{String}/V_{String,theo}$ .....	62

## IV. List of Tables

Table 3-1 General information about the Solar Park EHEU .....	26
Table 3-2 General information about the Solar Park FOR .....	28
Table 3-3 General information about the Solar Park HAI .....	30
Table 3-4 General information about the Solar Park RICH .....	32
Table 3-5 General information about the Solar Park KAL .....	33
Table 3-6 General information about the Solar Park HAL .....	35
Table 3-7 General information about the Solar Park FREI .....	36
Table 3-8 General information about the Solar Park EGG .....	38
Table 3-9 General information about the Solar Park AHL .....	40
Table 3-10 General information about the Solar Park ROHR .....	43
Table 3-11 General information about the Solar Park ELS .....	45
Table 3-12 Overview of PVPB & installation costs .....	47
Table 4-1 Results of all solar parks .....	58
Table 4-2 Voltage measurement example values .....	61
Table 4-3 calculation of potential yield gain per year and break-even point .....	63
Table 4-4 Future costs for the installation of further PVPB .....	66



## V. List of Abbreviation

alternating current .....	<i>AC</i>
anti-reflective coating .....	<i>ARC</i>
direct current .....	<i>DC</i>
ethylene-vinyl acetate .....	<i>EVA</i>
junction box .....	<i>JB</i>
Light-Induced Degradation .....	<i>LID</i>
maximum power point .....	<i>MPP</i>
maximum power point voltage .....	<i>V<sub>mpp</sub></i>
photovoltaics power booster .....	<i>PVPB</i>
PID-shunting .....	<i>PID-s</i>
potential induced degradation .....	<i>PID</i>
Renewable Energy Sources Act .....	<i>EEG</i>

### 1. Introduction

Man-made climate change is inevitable and one of humanity's biggest problems today [1]. The reason is simple, vast amounts of greenhouse gases are emitted into the atmosphere. These greenhouse gases trap heat, increasing the earth's average surface temperature. The more greenhouse gases there are in the atmosphere, the more the temperature rises. As the temperature rises, living conditions on earth become increasingly challenging and harsh for humans [2].

The greenhouse gases responsible for climate change are generated in various sectors, such as energy supply, transport, industry, and agriculture. In 2020, 16% of all greenhouse gas emissions in Germany were caused by electricity and heat production in coal-fired power plants alone [3]. Therefore, it is crucial that electricity production in coal-fired power plants is replaced by renewable energy production in, for example, photovoltaic power plants.

To replace coal-based power generation with renewable power generation as quickly and efficiently as possible, it is necessary to fully exploit the technological and economic potential of technologies such as photovoltaics. It is therefore essential to understand and consider degradation effects in photovoltaic modules. In addition to light-induced degradation (LID), which occurs mainly in the first hours of solar irradiation [4], there is also potential induced degradation (PID), which can lead to long-term shear defects in PV modules [5].

This master thesis aims to determine the influence of the PID effect on a portfolio consisting of several multi-megawatt free-field solar parks. Furthermore, it investigates how this effect can be prevented, reduced, or reversed.

The following thesis is divided into six main chapters. In the beginning, the introduction and the necessary theoretical basics are presented, which clarify the most important characteristics of power generation in solar parks with a focus on the effect of potential induced degradation.

It is followed by the material and methods chapter, which first deals with a market overview of the available technologies for avoiding and reversing the PID effect. Subsequently, the installation location of the selected technology to avoid the PID effect is presented. In addition, all solar parks equipped with this anti-PID technology are presented. A cost overview and a description of the analysis method follow.

In the fourth chapter, the results of the analyses are presented, as well as an illustration of the measurement results of the self-performed voltage measurement, which was carried out in the context of this thesis. Moreover, a short economic evaluation is given, with a comparison of the costs and the additional yield achieved.

The discussion chapter contains the evaluation and assessment of the results. Possible sources of error and causes are identified, and personal safety is discussed. Furthermore, there is an outlook on how the situation will develop in the future.

The last and concluding chapter contains the summary.

## 2. Fundamentals

The following chapter describes all necessary theoretical basics to understand the PID effect and how it affects the photovoltaic modules.

### 2.1 Photoelectric Effect

In solar cells, sunlight is converted directly into electrical energy. The principle is based on the photoelectric effect, more precisely on the internal photoelectric effect, which was discovered by Becquerel in 1839 and first described by Albert Einstein in 1905. Based on Bohr's atomic model, there are several energy bands in an atom on which the electrons of an atom can move around the nucleus. The band closest to the nucleus can hold two electrons. The subsequent bands can hold 8, 18, 32, 50, and continuing electrons. The top band which is completely filled is called the valence band. The next higher band can either be partially filled with electrons or contain no electrons. It is called the conduction band. The space between the conduction and valence bands is called the forbidden zone [6].

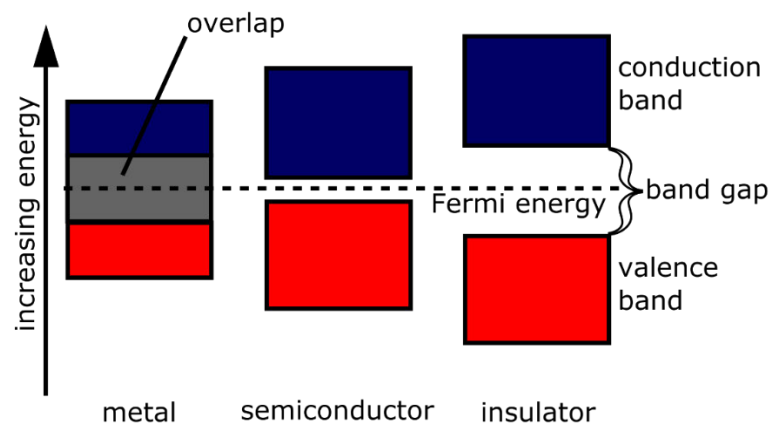


Figure 2-1 bandgap diagram [7]

A substance can be considered an insulator, semiconductor, or conductor depending on the occupation and arrangement of the bands (see Figure 2-1). The conduction band must contain electrons or overlap with the valence band for a substance to conduct. In an insulator, the bandgap between the conduction and valence bands is so large that it is challenging to lift an electron onto the conduction band. In a semiconductor, on the other hand, the conduction band is not occupied by electrons. However, the bandgap is relatively small. Thus, the lifting of electrons onto the conduction band is possible through the influence of radiation. Despite that, it is crucial with how much energy a photon hits an electron in the valence band. Photons need at least the energy required to lift an electron into the conduction band. If the energy is

too large, the electron is lifted into the conduction band but falls back to the conduction band edge, which results in the loss of energy in the form of heat dissipation. The opposite happens when the energy of the photon is too small. Then, the electron cannot be lifted into the conduction band. Hence, a specific wavelength is required, depending on the semiconductor material [6].

## 2.2 Electrical Description of Real Solar Cells

To illustrate the real solar cell in an equivalent circuit, we use the single-diode model shown in Figure 2-2. Together with the diode, the current source represents the solar cell itself. The serial resistance  $R_S$  describes the ohmic losses in the front contacts and the transitions between semiconductor and metal. The parallel resistance  $R_P$  describes leakage currents at the edges of the solar cell and all possible points which cause short circuits at the internal p-n junction [8].

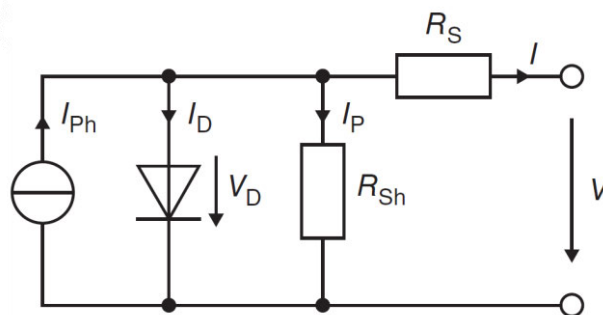


Figure 2-2 Single-diode model of a solar cell [8]

In order to develop an understanding of how  $R_S$  and  $R_{Sh}$  affect the characteristic curve of a PV module, it is necessary to obtain the characteristic curve of the model. Kirchoff's rules are first applied in Formula 2.1.

$$I = I_{Ph} - I_D - I_P \quad (2.1)$$

Together with the Formula for  $I_P$  (2.2) and the Shockley equation (2.3), the characteristic curve equation of the standard model (2.4) can be formed. ( $m$ =emmission coefficient;  $V_T$ =temperature voltage)

$$I_P = \frac{V_D}{R_{Sh}} = \frac{V + I * R_S}{R_{Sh}} \quad (2.2)$$

$$I_D = I_S * \left( e^{\frac{V+I*R_S}{m*V_T}} - 1 \right) \quad (2.3)$$

$$I = I_{ph} - I_S * \left( e^{\frac{V+I*R_S}{m*V_T}} - 1 \right) - \frac{V + I * R_S}{R_{Sh}} \quad (2.4)$$

Using the equation for I (2.4), the influence of the serial and shunt resistance on the IV characteristic curve can be shown. Figure 2-3 shows the influence of the serial resistance. It can be seen that with a larger serial resistance, the curve becomes flatter, and the fill factor thus decreases. Figure 2-4 shows the influence of the shunt resistance. When the resistance value of  $R_{Sh}$  becomes smaller, the fill factor also becomes smaller. Even the open circuit voltage is affected because the diode voltage  $V_D$  decreases with a larger  $I_p$ .

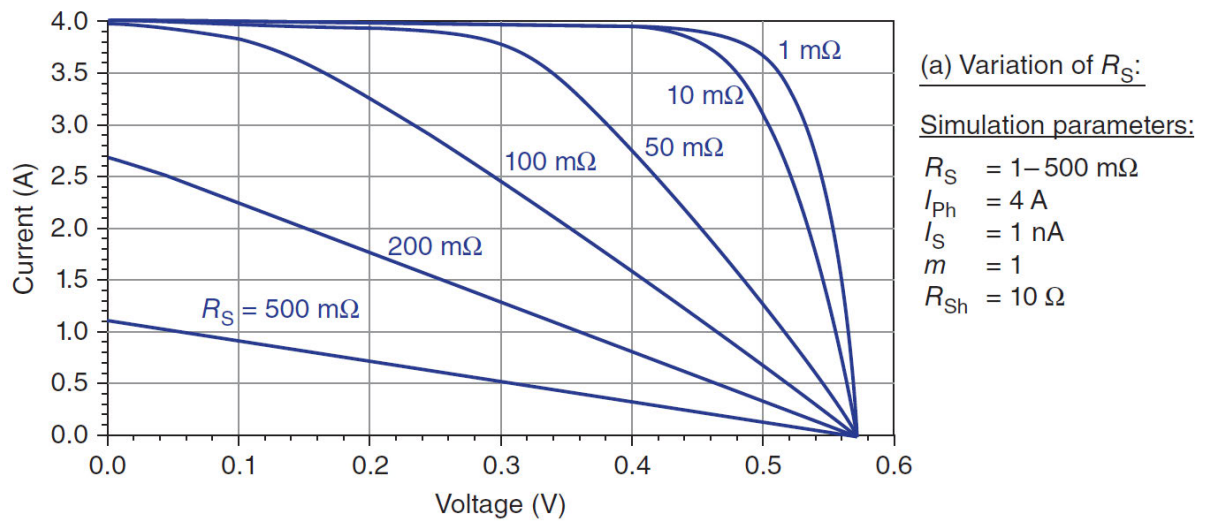


Figure 2-3 Influence of series resistance  $R_S$  on the solar cell characteristic curve [8]

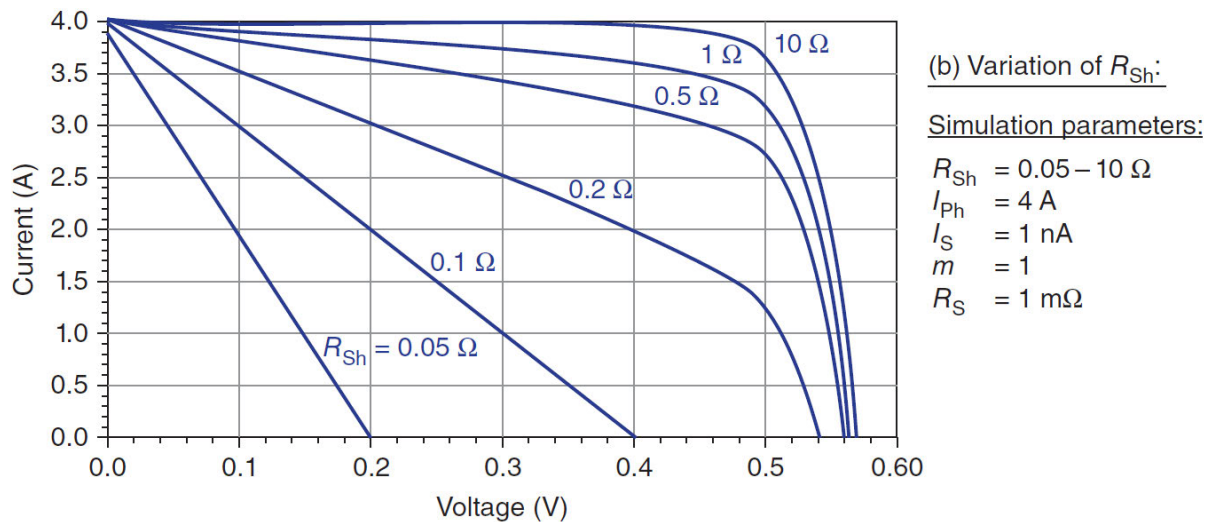


Figure 2-4 Influence of shunt resistance  $R_{Sh}$  on the solar cell characteristic curve [8]

### 2.3 Structure of a Solar Cell

The main component in a solar cell is the p-n junction, as it is also in a photodiode. A p-n junction, as the name suggests, is located between an n-doped and a p-doped semiconductor layer. In the case of an III-V crystalline silicon solar cell, the n-doped layer contains elements from the fifth main group in the periodic table, such as phosphorus. The n-doped layer is called the emitter. The p-doped layer contains elements from the third main group from the periodic table, such as boron or gallium, and is called the base. The general structure of a solar cell can be seen in Figure 2-5. The back contact is at the bottom, which represents the positive pole. The first semiconductor layer is often a p-doped layer connected to the back contact. Above the p-doped layer, there is the n-doped layer. On top of the n-doped layer are the front contacts, which represent the negative pole.

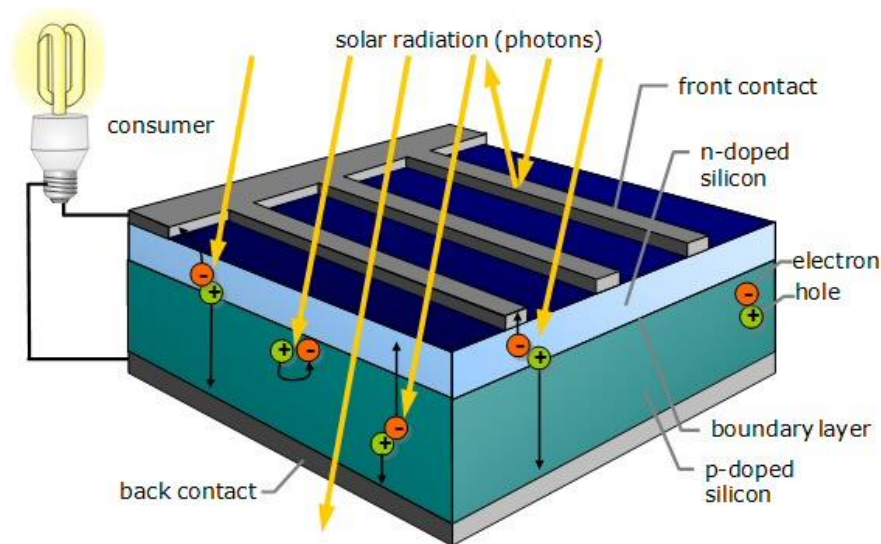


Figure 2-5 Structure of a solar cell [9]

At the boundary layer between the n- and p-doped semiconductor, a space charge zone is formed, as it is displayed in Figure 2-6. The free electrons in the n-doped layer move to some extent into the p-doped layer, and the holes from the p-doped layer move into the n-doped layer until the space charge region stabilizes. Therefore an electric field at the p-n junction is built.

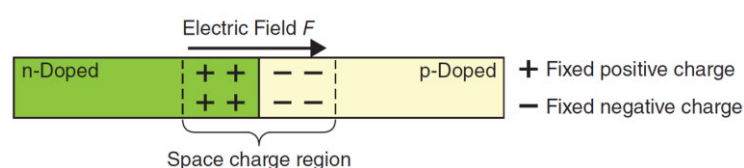


Figure 2-6 space charge region at the p-n junction [8]

When light hits the cell, each absorbed photon creates an electron-hole pair which is separated by the space charge region. The holes are transported through the base to the rear contact at the bottom, and the electrons through the emitter to the front contacts. The front contacts are realized by narrow metal strips, which collect the electrons as a current collector [10].

## 2.4 Structure of a Photovoltaic Module

The market for photovoltaic modules is vast, and there are various designs. A photovoltaic module is composed of multiple smaller solar cells, which are all electrically connected in series. In general, a solar module consists of 60 solar cells in one module. However, there are also modules with 72 cells or other amounts. Due to the serial connection, the voltages of the individual cells add up, thus the entire module has a significantly higher output voltage than a single solar cell. In Figure 2-7, an exemplary structure of a module is depicted. The numbering of the cells in the figure shows how they are connected. The cells are connected in series from number 1 to number 60. There are three bypass diodes on the top side, which ensure that, if the module is shaded, the shaded area within a string can be skipped and thus does not prevent the current flow in the entire string. The connections and the bypass diodes are almost always located on the back of the module in a so-called junction box (JB) [11].

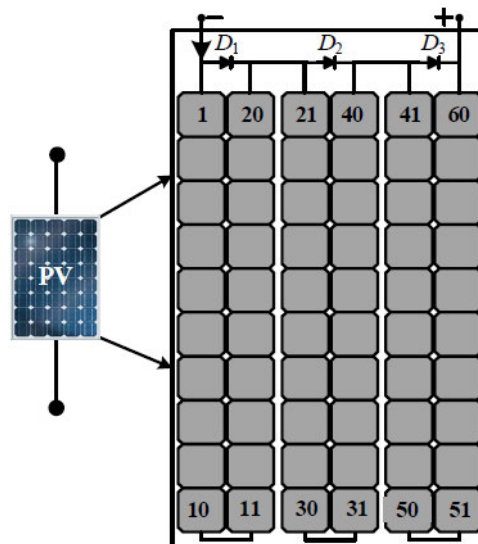
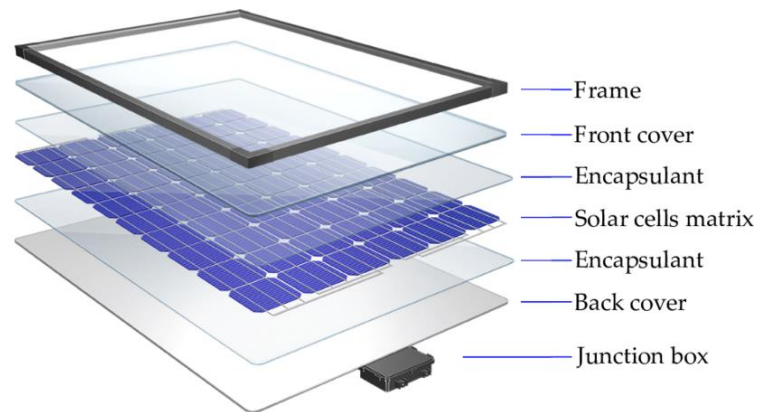


Figure 2-7 Schematic structure of a photovoltaic module [11]

Several protective layers protect the individual solar cells in a module from external environmental influences. These protective layers include the front glass, encapsulant, back



sheet, junction box, and module frame. The structural elements of a module are shown in Figure 2-8.



*Figure 2-8 Structural components of a photovoltaic module [12]*

The top layer is the front glass, which provides mechanical protection against environmental influences and, at the same time, must have a high transmittance so that the broadest possible spectrum of absorbable light can pass through. Normally soda-lime glass is used for the front glass. The soda-lime glass is easy to melt and mold, chemically stable, and inexpensive. The exact composition may differ based on the manufacturer. The typical composition of the glass is: 73%  $\text{SiO}_2$  – 15%  $\text{Na}_2\text{O}$  – 7%  $\text{CaO}$  – 4%  $\text{MgO}$  – 1%  $\text{Al}_2\text{O}_3$  [13, 14].

The actual solar cells are encapsulated in a polymeric material that protects the solar cells from moisture and other mechanical influences. The encapsulate usually consists of ethylene-vinyl acetate (EVA) [15].

On the actual photovoltaic cell, but still enclosed by the encapsulant, is the anti-reflective coating (ARC), which is not shown in Figure 2-8. The ARC can be made of  $\text{SiN}$  or  $\text{SiO}_2$ , for example, and can further include additional materials that enhance the anti-reflective property. However, the ARC does not necessarily have to be enclosed by the encapsulant. The ARC can also be applied subsequently to the upper surface of the glass, even when it is already installed. This way, existing PV parks can be retroactively equipped with ARC technology [16, 17].

The back sheet protects the module from UV radiation, moisture, wind, dust, and other chemicals on the backside. It is usually made of a composite material of PET-Tedlar film.

The junction box is usually located on the back of a solar module and protects the connections of the string cables and the bypass diodes.

The last and essential component is the aluminum module frame, which gives the module mechanical stability [18].

## 2.5 Structure of a Solar Park

In general, a solar park consists of photovoltaic modules connected in strings, which are connected to inverters that convert the direct current (DC) into alternating current (AC) to feed it into the public electricity grid. After the inversion process, the AC voltage is transformed with the help of transformers onto a higher voltage level of 20 kV. Following the stepping up of the voltage, the generated AC current can be fed directly into the medium- or high-voltage grid.

The fundamental structure of the module arrays consists of several modules connected in series to form a string, resulting in an operating voltage within the permissible voltages of the inverters used. Multiple strings are connected in parallel to one inverter, which leads to higher operating currents. This is limited by the maximum current per maximum power point tracker (MPP) tracker. Furthermore, the DC/AC ratio is intentionally often exceeded with its connected DC power. It can be as high as 1.3, meaning that 1.3 times as much DC power is connected to an inverter as the nominative AC power rating. However, the maximum permissible connected DC power is not exceeded, and the inverter limits are always regarded.

For the construction of multi-megawatt ground-mounted solar parks, there are essentially two concepts of how the parks inverter concepts can be constructed. Firstly, central inverters can be used. If central inverters are used, the strings are combined in generator junction boxes while still in the module field so that several smaller DC cables are combined into one cable with a larger cross-section. The cable with the larger cross-section then runs out of the field to the respective central inverter station. A general concept for central inverters can be seen in Figure 2-9 [10].

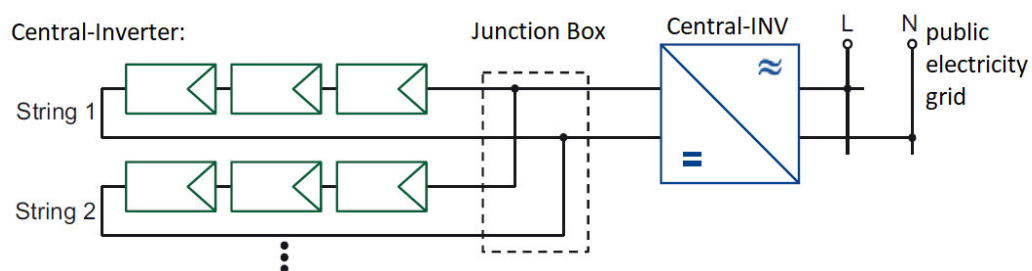


Figure 2-9 Concept of central inverters [10]

On the other hand, in a string inverter layout, the inverters are usually attached to the module tables themselves, which keeps the cable routes for the PV strings short and often allows them to be connected directly to the inverter without first being merged in junction boxes. In Figure 2-10, the general concept of string inverters can be seen [10].

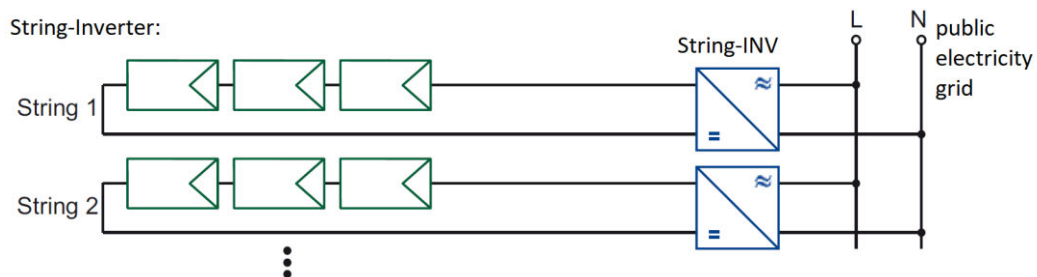


Figure 2-10 Concept of string inverter [10]

The electrical DC side of a solar park is usually set up as an IT network, which is not earthed at any point in the DC circuit. Nevertheless, the module tables and all other components that can be touched freely are grounded for plant safety. The absence of a pole grounding has two distinct advantages. First, personal safety is increased, as it is necessary to touch two live parts of different potential (e.g., plus and minus pole) to receive an electric shock. On the other hand, this enables the detection of ground faults. Thus, the DC grid is an isolated one with a two-fault safety when monitored.

In contrast, there is the system grounding of one pole, either the plus or the minus pole, with the minus pole practically always being the pole to be grounded, as it is common in solar parks with thin-film modules [19]. In this case, it is sufficient to touch only one live part to receive an electric shock. In addition, it is not possible to detect an earth fault. However, grounding the negative terminal can positively affect the PID effect, which will be discussed in detail later. Thus, in some solar parks, reduced plant safety is accepted in order to prevent the PID effect. However, there are also hybrid approaches in which the system grounding of the negative pole can be temporarily removed or added. For example, grounding can be removed when the intrusion detection system detects human entry into the solar farm. Another approach is to connect the grounding only at night while the solar modules are not producing electricity and then remove the grounding during the day [20].

Currently, many solar parks are still designed with a system voltage of 1000 V. However, the increase of the system voltage to 1500 V and even 2000 V is already underway and brings some advantages. The increased DC voltage means that the strings can contain more modules

in series and therefore reduce the number of strings in total. This will save wiring costs and require less auxiliary equipment by reducing the number of generator junction boxes needed, if any, and the number of fuses [21, 22].

### 2.6 Potential Induced Degradation

In solar energy systems that use photovoltaic technology, the potential induced degradation, or the PID-effect, is a common phenomenon. The potential induced degradation includes all degradations of a solar module, which are caused by a different potential between the semiconductor and the external components of the module [23]. If the modules are affected by PID, they can lose up to 80% of their power in extreme cases. The loss of performance may appear over a long period of time, or it may appear only a few days or weeks after installation. An unplanned and significant reduction in output has detrimental effects on the economic viability of a solar park project, as yields fall, and thus the planned financing is threatened. However, the PID effect can be prevented and even reversed [24]. The following work mainly focuses on the PID effect of the type PID-shunting, which is abbreviated PID-s to distinguish it from other forms of PID. Other types of PID are the corrosion of transparent conductive oxide layers in thin-film modules and the dissolution of the anti-reflective coating or the degradation of metallization in crystalline Si solar modules [25]. PID-s is the most widespread and most harmful version of PID and is therefore of prime importance.

PID is caused by small unwanted currents between the module frame, the glass, the anti-reflective coating on one side, and the solar cell's semiconductor on the other side. The degradation process is related to the migration of sodium ions from the glass through the encapsulation and the anti-reflective coating into the cell. The penetration of the ions into the solar cell massively reduces the parallel resistance of the cell, which is also called shunting. The degradation of the parallel resistance in the cell causes a reduction of the fill factor and thus decreases the power output, as it can be seen in Figure 2-4. At very high levels of PID-s, the open-circuit voltage  $V_{OC}$  and the short circuit current  $I_{SC}$  can also be degraded due to internal short-circuiting [25]. The reason for the ion movement are potential differences between the cell and the module frame or glass. The sodium ions are positively charged and are thus attracted by a negative pole. If the module field is not grounded and no other measures have been taken to prevent PID, it is possible that some of the cells in the photovoltaic modules, or even all of the modules, have a negative voltage with respect to

ground. The effect becomes larger when the cell has a higher negative potential with respect to earth [17, 24, 26].

It is also known that environmental influences can enhance the PID effect. These include temperature and humidity [24]. However, these factors cannot be influenced and are therefore not considered in detail in this thesis.

As already mentioned, the effect depends on how large the negative voltage of the cells against the ground is. Therefore, it is essential where the modules are located in the string. For example, if we assume that the positive pole has a potential of 0V, then the module closest to the positive pole has the smallest negative voltage to ground. The module farthest from the positive pole, i.e., closest to the negative pole, has the highest negative voltage against ground and thus the highest risk for PID occurrence [24]. An exemplary representation of the string voltage can be seen in Figure 2-11.

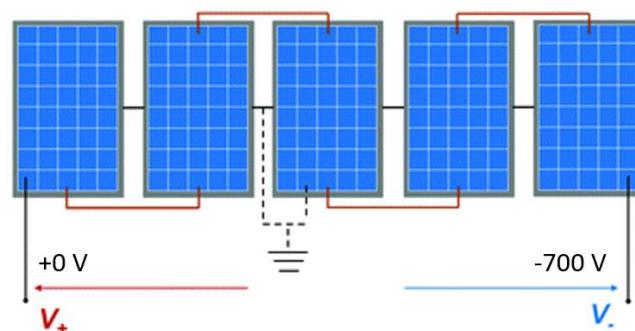


Figure 2-11 Exemplary depiction of a string voltage [27]

However, the magnitude of the negative potential with respect to ground also depends on the topology of the inverters. The inverters often divide the voltage symmetrically with respect to ground, thus allowing a negative voltage to be applied to the modules with respect to ground. Inverters with transformers can be grounded, which means that the voltage can be permanently raised to a potential above the ground potential. Figure 2-12 shows the voltage in relation to ground of various inverters from the manufacturer SMA. The lower blue line represents the potential of the negative pole, and the upper red line the potential of the positive pole.

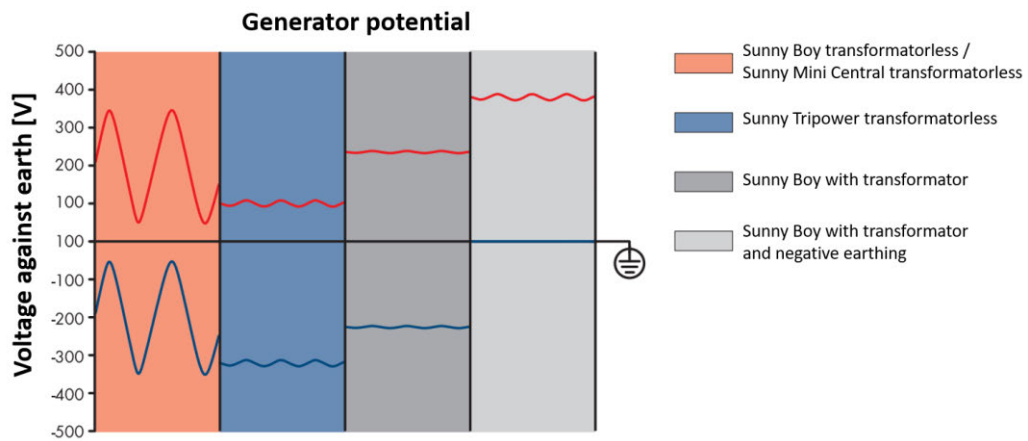


Figure 2-12 Generator potential example for an MPP voltage of 400V [28]

## 2.7 Detection of the PID Effect

The PID effect can be detected by observing the maximum power point voltage ( $V_{MPP}$ ), as the PID effect is most noticeable in the voltage. Differences in the MPP voltages in the modules of a string can indicate the presence of PID. There are several ways to detect PID [24].

First, the IV curve of the modules or the strings can be measured. In IV curve measurement, the current-voltage curve of a module or string is measured. This way, modules or strings with low voltage or power values can be identified [24]. The PID effect causes a reduction of the parallel resistance of the solar cell and a slight degradation of the short circuit current  $I_{SC}$ , as shown in Figure 2-4. In Figure 2-13, an electroluminescence image can be seen showing different degrees of degradation on individual module cells. The graph shows the individual IV characteristic measurements of the cells in the top two strings, demonstrating the evolution of PID from only minor damage and diode-like behavior to a near ohmic resistance characteristic [29].

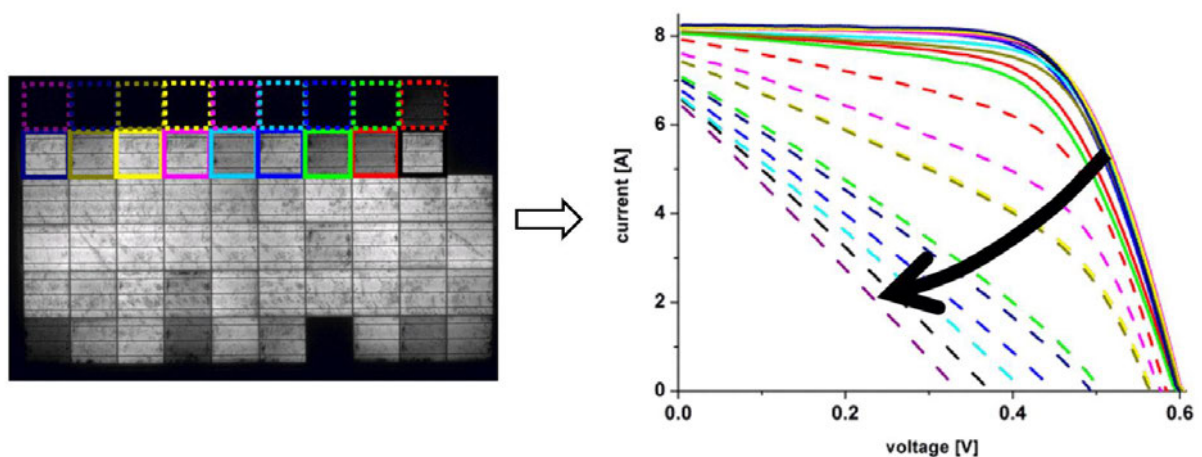


Figure 2-13 EL image of a PID affected module (left) and I-V characteristic of individual cells [29]

However, it should be noted that when IV curve measurements are performed on entire strings in the solar farm, the power reduction is primarily reflected in a reduction of the open-circuit voltage. This is because bypass diodes in the modules can bypass the defective substrings of a module when the degradation effect becomes too strong, as described in Chapter 2.4. Figure 2-14 shows the IV-curve measurements of an example plant affected by PID. It can be seen that reductions can be found mainly in the open-circuit voltage [29].

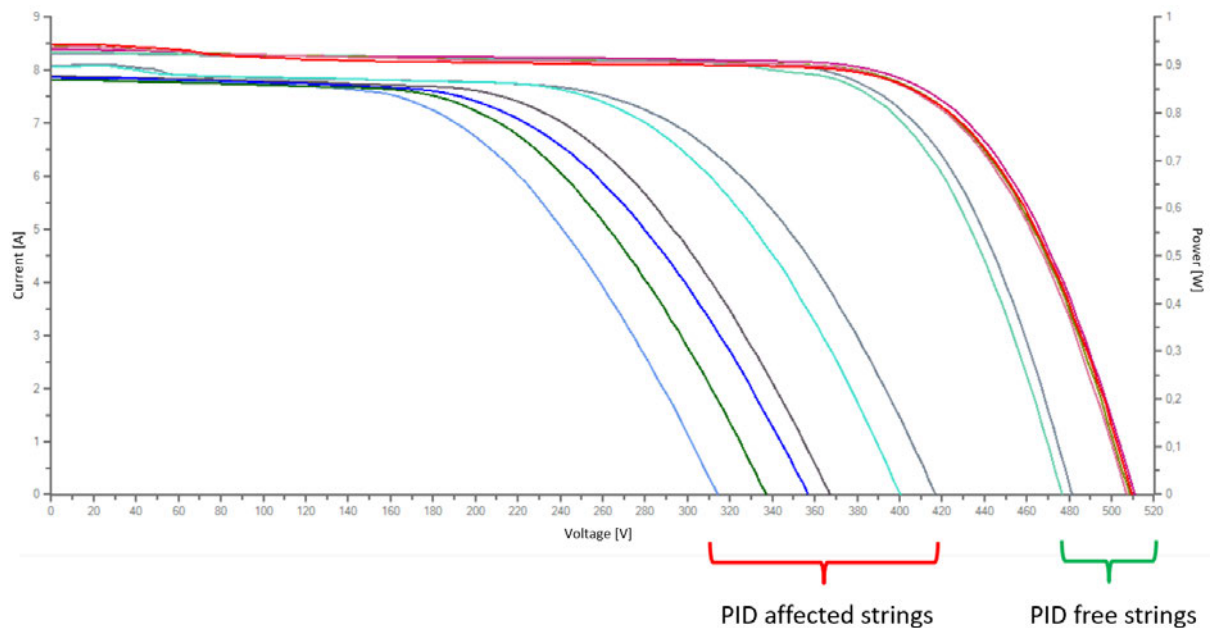


Figure 2-14 string IV-curve measurements of an example solar energy system which is affected by PID [29]

In addition, an electroluminescence measurement can be made in which PID affected modules glow dark. Electroluminescence is an optical and electrical phenomenon in which material emits light due to electric current. Starting at the negative side of a string, the modules and cells affected by PID can thus be easily identified by a dark coloring. Figure 2-15 shows an example of this [24].

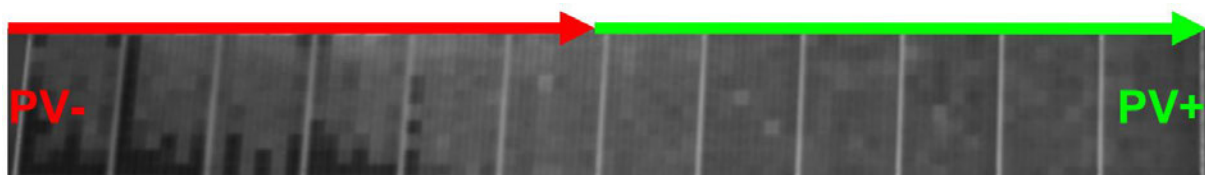


Figure 2-15 EL image of a floating PID string with degraded panels on the side with negative potential [30]

Another measurement is the thermography of the modules, which can determine the temperature of the modules. Here, the effect that modules affected by PID are heated up is exploited [24]. In Figure 2-16, the comparison between an electroluminescence image and a



thermographic image of a module affected by PID can be seen. Especially the cells at the edge and thus close to the module frame are heated up, which is characteristic for PID [26].

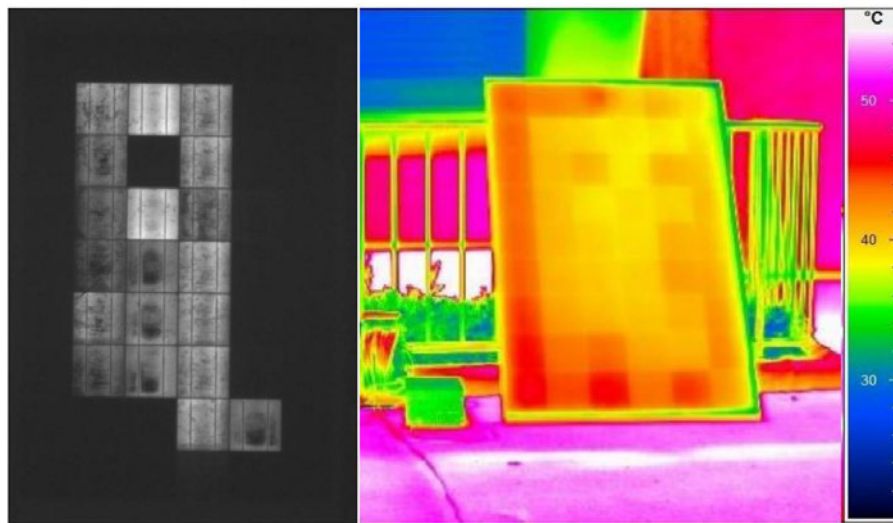


Figure 2-16 electroluminescence (left) and thermographic (right) image of a with PID affected module [26]

The TS IEC 62804-1:2015-08 standard was created to standardize the test procedures for PID detection. IEC 62804-1 defines two standardized test methods that can be used to measure the potential induced degradation of individual modules. The tests are intended to evaluate the sensitivity of PV modules to PID regardless of the actual stresses under which they operate in different climates and systems.

TS IEC 62804-1:2015-08 also states that solar modules that pass the test procedure with a power deviation of less than 5% can be labeled as PID-free [31]. Typically, with regard to the modules, PID was not mentioned before the introduction of this standard because the manufacturers would have made themselves vulnerable when labeling PID-free, and then PID appeared. With the introduction of the standard, module manufacturers can now more easily label their modules as PID-free. However, power reductions of up to 5% can still occur.

For example, the solar module 'Q.Plus L-G4.2 340-350' is declared as PID resistant, see Figure 2-17. However, reference is made to the test methodology of IEC 62804, and thus a performance loss of up to 5% is possible. The corresponding data sheet is attached in A2-7-1.



### ENDURING HIGH PERFORMANCE

Long-term yield security with Anti-PID Technology<sup>1</sup>, Hot-Spot-Protect and Traceable Quality Tra.Q™.

<sup>1</sup> APT test conditions according to IEC/TS 62804-1:2015, method B (-1500V, 168h)

Figure 2-17 Q.Plus L-G4.2 Anti-PID Feature



## 2.8 Prevention and Inversion of the PID-effect

Different approaches can be taken to prevent the degradation through PID. In addition, there are also methods to reverse the PID effect.

Preventively, in order to reduce the amplification of the PID effect by environmental influences, a location can be selected where favorable environmental conditions prevail. Thus, places where the temperature and humidity are generally lower should be chosen. Topological sinks should be avoided. Furthermore, suppose a windy location is chosen. In that case, the wind cools the modules, causing them to have a lower temperature, positively affecting and reducing the PID effect and increasing the module's efficiency.

Moreover, PV modules can be built with PID-resistant material. However, this increases the costs since better and more expensive material has to be used for the anti-reflective coating or the front glass. For example, when chemically strengthened glass containing K<sup>+</sup> instead of Na<sup>+</sup> is used as front glass rather than classical soda-lime glass, no degradation of Si-crystalline modules was observed [13]. To understand how the material properties of the soda-lime glass, the encapsulant and the ARC affect the PID effect, the voltage divider model on module level is depicted in Figure 2-18.

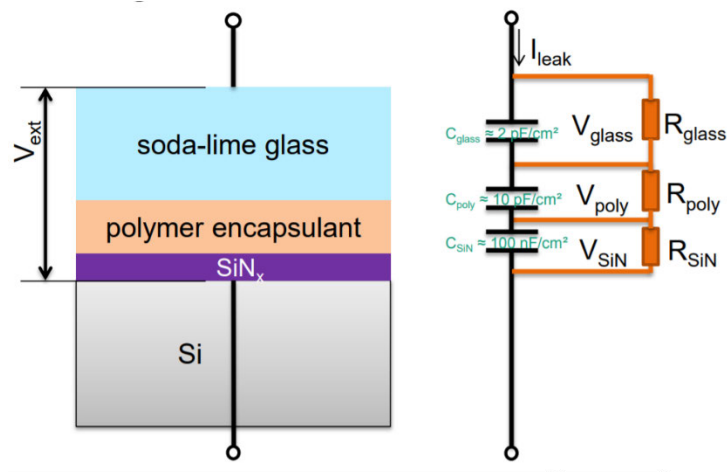


Figure 2-18 Voltage divider model for PID on module level [17]

The critical parameter for resistance against PID is the voltage across the ARC, which is the SiN<sub>x</sub> layer ( $V_{SiN}$ ). In order to obtain a Formula for  $V_{SiN}$ , Formula 2.6 is substituted into 2.5, resulting in Formula 2.7, which describes the voltage across the ARC [17].

$$V_{SiN} = I_{leak} * R_{SiN} \quad (2.5)$$

$$I_{leak} = \frac{V_{ext}}{R_{glass} + R_{poly} + R_{SiN}} \quad (2.6)$$

$$V_{SiN} = \frac{R_{SiN}}{R_{glass} + R_{poly} + R_{SiN}} * V_{ext} \quad (2.7)$$

Due to a lower  $V_{SiN}$  voltage, the Na ions experience a lower drift towards the semiconductor, thus weakening the PID effect. With reference to Formula 2.7, it can be seen that due to a high resistance in the glass ( $R_{glass}$ ) and in the polymer encapsulant ( $R_{poly}$ ), a lower voltage is applied across the ARC, which positively affects and reduces the PID effect [17].

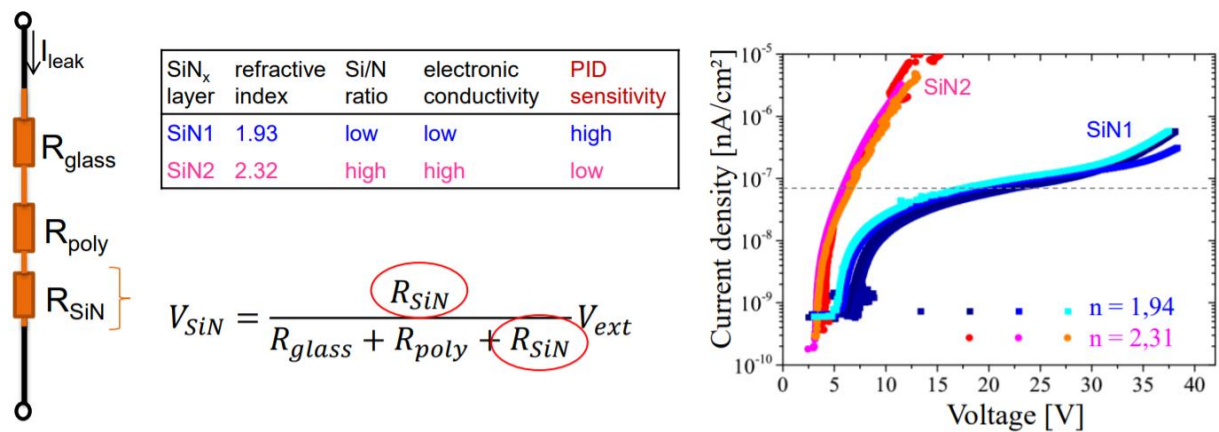


Figure 2-19 Measurement of the voltage across SiN<sub>x</sub> layer [17]

In Figure 2-19, the voltage measurement across the SiN<sub>x</sub> layer is depicted with two different kinds of the SiN<sub>x</sub> layer. Since the resistance of SiN<sub>x</sub> ( $R_{SiN}$ ) is much smaller than the resistance of the glass ( $R_{glass}$ ) and the encapsulant ( $R_{poly}$ ), the SiN<sub>x</sub> layer does not have a significant impact on the leakage current but the PID-s sensitivity [17].

Another possible method to prevent PID is to use a system grounding at the negative pole, leaving the module array with only positive voltages with respect to the ground potential. With this method, the negative side of the module field is grounded permanently or only partially. By grounding the negative pole side, negative voltages no longer occur between the module frame and the ground potential. No more positive ions can migrate into the module frame, thus preventing the PID effect. However, grounding only prevents the PID effect and cannot reverse it. Despite that, the grounding of a pole reduces the system safety since fault currents occur immediately in the event of a ground fault [32]. This also affects personal safety, as it is sufficient for a human to touch a live part to receive an electric shock. Furthermore, the negative side of the module field can only be grounded if the inverters support it [33].

A method that prevents the PID and can even reverse it is the application of a repair voltage to the module field overnight. This means that when the modules stop producing current after sunset and no voltage is present, a positive repair voltage is applied to the negative side of the module array. This causes the positive sodium ions that have already penetrated the cell to migrate partially back out of the solar cell and into the module frame/glass and can therefore reverse PID [24].

### 3. Materials and Methods

In the following chapter, the technology used to reverse the PID effect is described and all the solar farms studied are briefly presented. In addition, the following analysis method and the procedure for the field measurement carried out as part of this thesis are explained.

#### 3.1 Market Overview

As mentioned before, there are several methods to stop and reverse the PID effect. Since the portfolio in question already exists and has been built, selecting a suitable site with favorable environmental conditions is not an option. The system-wide grounding of the negative pole of the solar farm is not considered, as this would endanger personal safety and make it challenging to detect ground faults.

Another feasible option is to use inverters that already have a built-in anti-PID function. The inverters then automatically apply a positive voltage to the negative side of the module field after sunset. This voltage is often called and referred to as the repair voltage. However, the opportunity of buying new inverters is rarely available in an already built solar park since its costs would be too high. The currently installed inverters do not have a built-in anti-PID function. In this case, it is possible, for example, to repair individual inverter failures with new inverters that have a built-in anti-PID function. Furthermore, it is possible to carry out an inverter repowering in which new units replace all existing inverters of a solar park. Undoubtedly, this is a costly undertaking that makes economic sense in very few cases. Nevertheless, for poor-performing inverters that have a high failure rate and cause a non-negligible yield loss, this is a possibility. However, this case occurs very rarely and must then be examined individually.

Though, if a new solar park is built, there is the possibility to take advantage of purchasing and installing inverters that offer the option to reverse the PID effect initially. According to internal information from the portfolio owning company, the most used inverters at present are from the manufacturers Sungrow and Huawei. The latest models from Sungrow, such as the SG110CX, already integrate an anti-PID function, which applies a positive potential to the negative side of the module field at night [34]. Inverter manufacturer Huawei also already offers the sun2000-60ktl-m0, an inverter with a built-in anti-PID function [35].

However, replacing the existing inverters in the portfolio in question is not an option due to the stated economic reasons. A so-called float controller or an anti-PID box can be used to achieve PID protection or reversal in an existing plant, although these two variants differ slightly from each other [33, 36].

The principle of the float controller during the day can be seen in Figure 3-1. During the day, it sets the voltage of the entire installation above the ground potential. It thus prevents negative voltage from occurring with respect to ground. As a result, PID is prevented during the day.

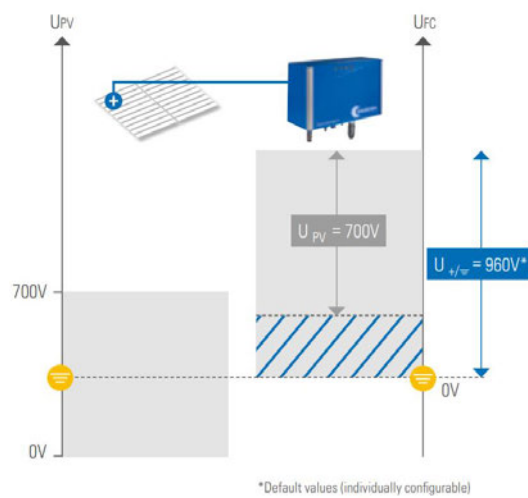


Figure 3-1 float controller day mode [36]

In addition, the float controller applies a repair voltage to the modules at night to reverse any PID effect that may have occurred previously. The principle of the float controller at night can be seen in Figure 3-2.

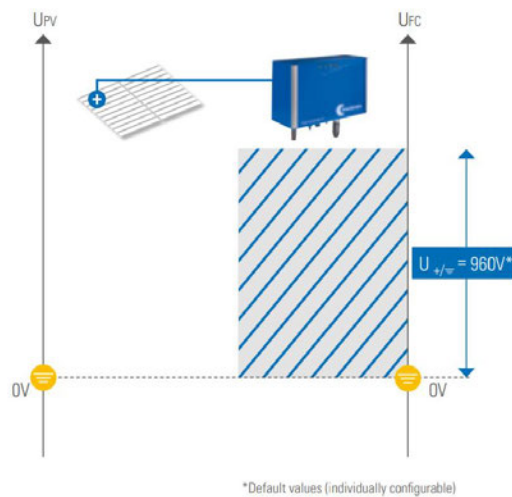


Figure 3-2 float controller night mode [36]

In contrast, the anti-PID boxes only apply a repair voltage at night and do not interfere with the plant operations during day time. As for the float controllers, several different manufacturers offer anti-PID boxes. However, for the portfolio-wide test, so-called Photovoltaic Power Boosters (PVPB) were used, offered by the company PV performance GmbH.

When the voltage of the module field falls below 30 V, the PV Power Booster boxes switch on and apply a positive voltage of approximately 700 V to the negative pole of the module field between the negative pole and ground as the manufacturer states it. When the voltage of the module field exceeds 60 V in the morning, the PV Power Booster Box switches off, and regular feed-in operation begins.

The PV Power Boosters are offered in different variants for string inverters and central inverters. The models 'PVPB SI 10-1 SL', 'PVPB SI 20-1 SL', and 'PVPB SI 30-3' are made for string inverters, whereby the first number indicates the current that can be applied to the module field in mA. The last number describes the number of inverters that can be connected to the PVPB.

The models 'PVPB CI 60-1', 'PVPB CI 60-3', and 'PVPB CI 60-1 SL' are made for central inverters. The naming scheme here is the same as for string inverters. [37] For illustration, a PVPB SI 30-3 is shown in Figure 3-3.



Figure 3-3 PVPB SI 30-3 [37]

If there are not enough connections available, a Power Extender can be connected to the Power Booster, adding additional connections for inverters. The Power Extender does not include any particular technology and, in principle, represents a busbar. It is connected to one

output of the PVPB and extends it by three additional outputs, making four connections available. An example image of a PVPB extender can be seen in Figure 3-4.



*Figure 3-4 PVPB Extender*

The anti-PID boxes or PV Power Booster boxes were chosen because the boxes can be tested free of charge during a six-month trial period.

### 3.2 Location of Installation

Since the PV Power Booster Box applies a repair voltage to the modules at night, the box must be connected directly to the module array on the DC side of the inverters. The basic design and connection of a PVPB is shown in Figure 3-5. It is important to note that, depending on the constellation of inverters, each negative pole of the module field, which is supposed to receive a repair voltage at night, is connected to the PVPB. In the case of three inverters, each connected separately to the module field, all negative lines are connected to the PVPB. On the positive side, however, only one line must be connected to the PVPB. In order to prevent short circuits and the associated fires, so-called inline fuses are installed on the DC cables connected to the incoming DC lines just before the connection point. These hang in the cable, contain a fuse, and connect via an MC4 plug. The PVPB also requires a 230V AC connection and a ground connection.

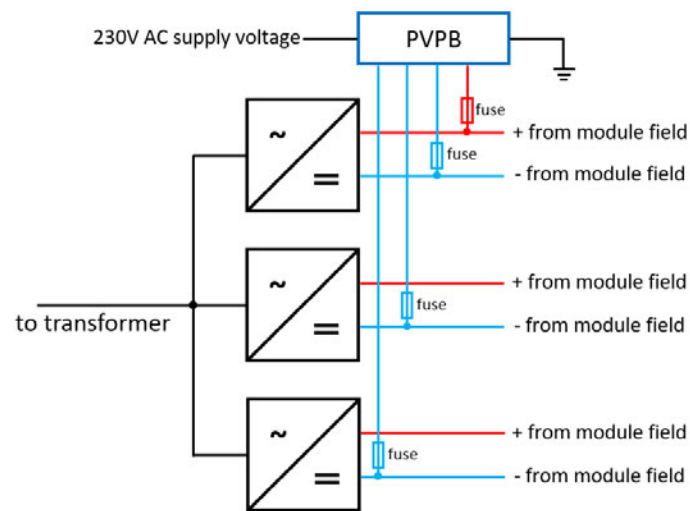
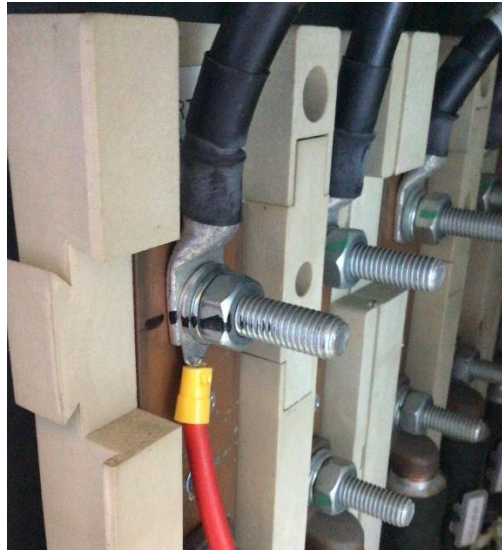


Figure 3-5 basic connection design of a PVPB (source: own illustration)

The first installation step for the PVPB is attaching the box to a wall near the inverters. Then, if the box is installed in a central inverter station, the grounding of the housing must be connected to the potential equalization rail of the inverter station. Afterward, the MC4 DC outputs PV1(+), and PV1(-) are connected to the inverter with the highest DC string voltage. Subsequently, the remaining DC cables are connected. Finally, the PVPB is connected to a 230V AC connection.

The solar cables from the PVPB to the inverters are usually laid in the station basement. In most cases, threaded holes or threaded pins are available on the DC busbar in front of central inverters for connecting the DC solar cables from the PVPB. The DC cables from the PVPB can then be attached to the DC busbar of the inverter using suitable ring terminals, screws, and nuts, as it can be seen in Figure 3-6.





*Figure 3-6 Connection of PVPB to DC busbar*

It should be noted that the schematic diagrams in the presentation of the solar parks do not include fuses, surge protectors, switches, number of cables, and cable cross-sections. Furthermore, on the DC side of the inverter, there is a minus and a plus side, but for the sake of clarity, these are not drawn separately from each other. The representation is only to clarify where the PVPB was connected.

### 3.3 Selection of Reference Inverter

In order to test the effectiveness of the PV Power Booster boxes, one or multiple inverters must be selected for each solar farm. The test inverters are selected in advance based on low yield values and low DC voltage compared to other inverters. The selected inverter or inverters are equipped with the PVPB. Care should be taken to ensure that the selected inverters and their associated DC areas are not exposed to shading during the test period.

### 3.4 Overview of the Portfolio

The following section briefly presents the solar farms that have been equipped or were planned to be equipped with a PVPB box. All solar parks are located in Germany. Basic information about each solar park is provided, including the geographical and topological location, the nominal power, the type of modules, the type of inverters, the general electrical structure, and the height of the feed-in tariff, which is granted by the Renewable Energy Sources Act (EEG). Inside the layout for the general electrical structure, the installation location for the PVPB is depicted.

Furthermore, results of past characteristic curve measurements are considered and compared with the expected degradation based on the performance guarantee to determine whether the solar park could be affected by the PID effect at all.

Typically, solar modules are given a performance guarantee, which guarantees that they will not fall below 90% of their stated rated power for the first ten or twelve years and 80% for the first 20 or 25 years. Some manufacturers only specify that the 90% may not be undercut in the first ten years, while others specify a linear degradation, with a specific guaranteed performance existing each year. Often, the performance guarantee starts with a value below 100% already in the first year. In order to calculate the power that the module must still have after  $x$  years of operation, linear regression can be used, as it is seen in Formula 3.1.

$$y = m * x + b \quad (3.1)$$

In order to avoid conclusions about the exact location of the solar park or the project company, the names of the solar parks were changed, and the exact location was not disclosed. All information of the solar parks were taken from the company's internal documentation and represents the current state of construction.

### 3.4.1 EHEU – Solar Park Bavaria North

The Solar Park EHEU is in the North of the German federal state Bavaria and is divided into five fields, as shown in Figure 3-7. The park is located between several agricultural fields, and some small shrubbery surrounds it. The topological environment is slightly hilly, and a small area of the solar park is in a depression.



Figure 3-7 Solar Park EHEU satellite picture [38]

The nominal power output sums up to 4,861.08 kWp. The commissioning date of the solar park is 30.06.2010, which results in a feed-in tariff of 0.2843 €/kWh. There are four central inverter stations, each containing an inverter of the type ‘SMA SC 1250 MV-11’. The installed modules consist of 13,392 Sunowe SF-175 and 13,608 Sunowe SF-185, made of monocrystalline silicon. The general information can be seen in Table 3-1.

Table 3-1 General information about the Solar Park EHEU

Solar Park EHEU	
Nominal DC power	4,861.08 kWp
Commissioning date	30.06.2010
Modul type	Monocrystalline
Modules	13,392 Sunowe SF-175 13,608 Sunowe SF-185
Inverter concept	Central inverter
Inverters	4x SMA SC 1250 MV-11
Feed-in tariff	0.2843 €/kWh

The measurement of the characteristic curve was carried out on 01.06.2021 and the commissioning date of the park is 30.06.2010. The module manufacturer gave a fixed

performance guarantee of 90% for the first ten years and 80% for the first 25 years, see Appendix A3-1-1. Accordingly, the modules must still have an output of above 80% in 2021. With linear regression, on the other hand, the modules should have an output of 89.33% in 2021 and may therefore be a maximum of 10.67% below their stated rated output. During the characteristic curve measurement, it was noticed that 289 of 501 measured strings performed worse than the maximum allowed -10.67% by the theoretical linearly considered performance guarantee, which could be due to PID.

For the test, the PVPB was installed in the central inverter station 2. The general installation layout can be seen in Figure 3-8. Each of the ‘SMA SC 1250 MV-11’ inverter station's inverter units consists of two smaller inverter units. The PV array is connected via a DC-busbar at each subunit.

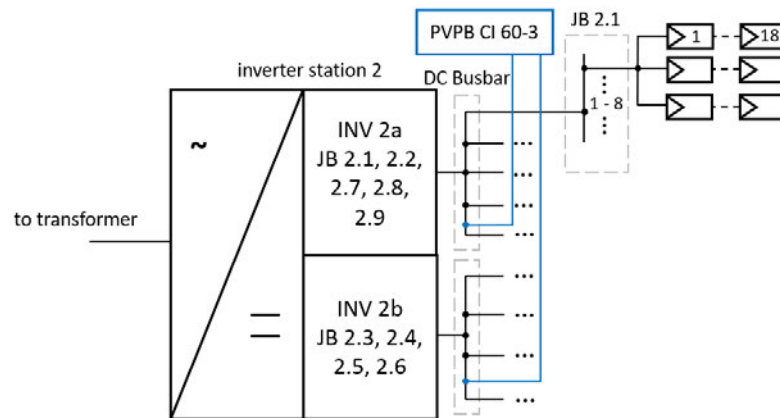


Figure 3-8 schematics of the PVPB installation in the solar park EHEU (source: own illustration)

### 3.4.2 FOR – Solar Park Brandenburg East

The Solar Park FOR is in the east of Brandenburg, close to the border of Poland. As shown in Figure 3-9, the Solar Park is divided into two fields. The park is topologically located on one plain level and is adjacent to a residential area on three sides. On the southern side, there is a flat meadow.



Figure 3-9 Solar Park FOR satellite picture [38]

The Solar Park has a rated DC power output of 3,691.38 kWp. It was commissioned on 27.03.2012 and therefore has a feed-in tariff of 0.2111 €/kWh. The used modules are CandianSolar CS6P 235P, of which there are 15,708 pieces. The module type is polycrystalline. The inverter layout comprises two central inverter stations, with the first station containing five ‘Power-One PVI-330.0-TL’ and one ‘Power-One PVI-220.0-TL’ inverter. The second station contains four ‘Power-One PVI-330.0-TL’ inverters. The general information can also be seen in Table 3-2.

Table 3-2 General information about the Solar Park FOR

Solar Park FOR	
Nominal DC power	3,691.38 kWp
Commissioning date	27.03.2012
Modul type	Polycrystalline
Modules	15,708 CanadianSolar CS6P 235P
Inverter concept	Central inverter
Inverters	9x Power-One PVI-330.0-TL 1x Power-One PVI 220.0-TL
Feed-in tariff	0.2111 €/kWh

No characteristic curve measurement was carried out for the Solar Park FOR. Therefore, no statement can be made about the degree of degradation of the modules.

The PID Booster Box was installed at the inverter E03 in station 1. Inverter E03 is a ‘PVI-330.0-TL’ rack composed of six ‘PVI-55.0-TL-DE’ inverter units. The entire E03 rack is connected to a common DC busbar. The solar modules are connected to the busbar via a junction box and a DC combiner. The PID Booster Box was connected to the DC busbar, which allows the entire module array connected to E03 to be supplied with the repair voltage at night. A schematic representation of the interconnection can be seen in Figure 3-10.

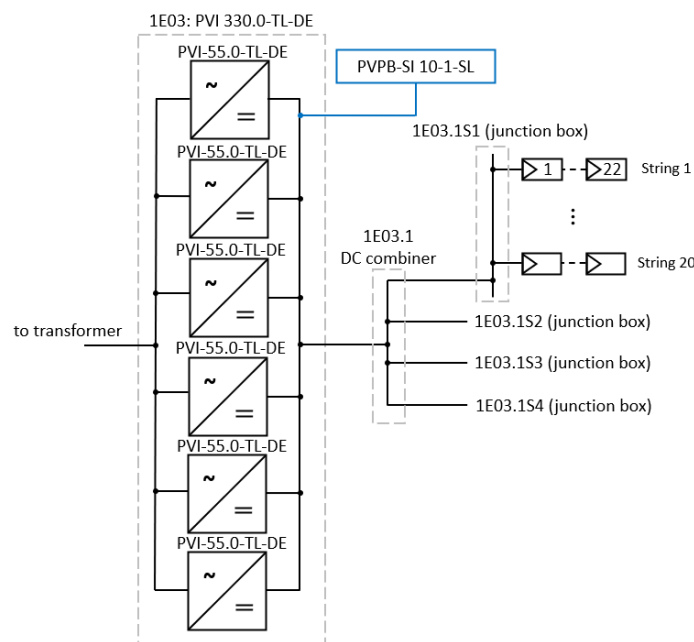


Figure 3-10 schematics of the PVPB installation in the solar park FOR (source: own illustration)

### 3.4.3 HAI – Solar Park Bayreuth

The Solar Park HAI is located close to Bayreuth in the State of Bavaria. The solar park is located on a slope, with the park's southern side in the valley floor. However, north of the solar park HAI is another solar park, which is not part of the investigation. Otherwise, the solar park is surrounded by fields and by some smaller bushes along the fence. The location and the satellite picture of the Solar Park HAI can be seen in Figure 3-11.



Figure 3-11 Solar Park HAI satellite picture [38]

The Solar Park has a rated DC power output of 3,196.80 kWp. It was commissioned on 21.06.2010 and therefore has a feed-in tariff of 0.2843 €/kWh. The used modules are Sunowe SF 125\*125-72-M (185 Wp), of which there are 17,385 pieces. The module type is monocrystalline. The inverter layout is made of three central inverter stations, with each of the stations containing six ‘Aurora PVI Central 300 TL’ inverters. The general information are summarised in Table 3-3.

Table 3-3 General information about the Solar Park HAI

Solar Park HAI	
Nominal DC power	3,196.80 kWp
Commissioning date	21.06.2010
Modul type	Monocrystalline
Modules	17,385 Sunowe SF 125*125-72-M (185 Wp)
Inverter concept	Central inverter
Inverters	9x Aurora PVI Central 300 TL
Feed-in tariff	0.2843 €/kWh

The characteristic curve measurement was carried out on 20.04.2020, and the commissioning date of the park is 21.06.2010. The module manufacturer gave a fixed performance guarantee of 90% for the first twelve years and 80% for the first 25 years, see Appendix A3-3-1. Accordingly, the modules must still have an output of above 90% in 2020 and may therefore be a maximum of 10% below their stated rated output. During the characteristic curve



measurement, it was noticed that none of the 40 measured modules performed worse than the maximum allowed -10% by the performance guarantee.

The PVPB box was installed at inverter 10 in station 3. Inverter 10 is a ‘PVI-300-TL’ rack composed of six 55 kW inverter modules. Each 55 kW module is connected to a subarea of the module field. Every subarea consists of 20 strings à 16 modules, which are combined in a junction box in the module field. There is a DC cable running from the junction box to the inverter. Since there are six individual connections to the module field for each rack, only three of the inverter modules can be equipped with a PVPB. A schematic representation of the interconnection can be seen in Figure 3-12.

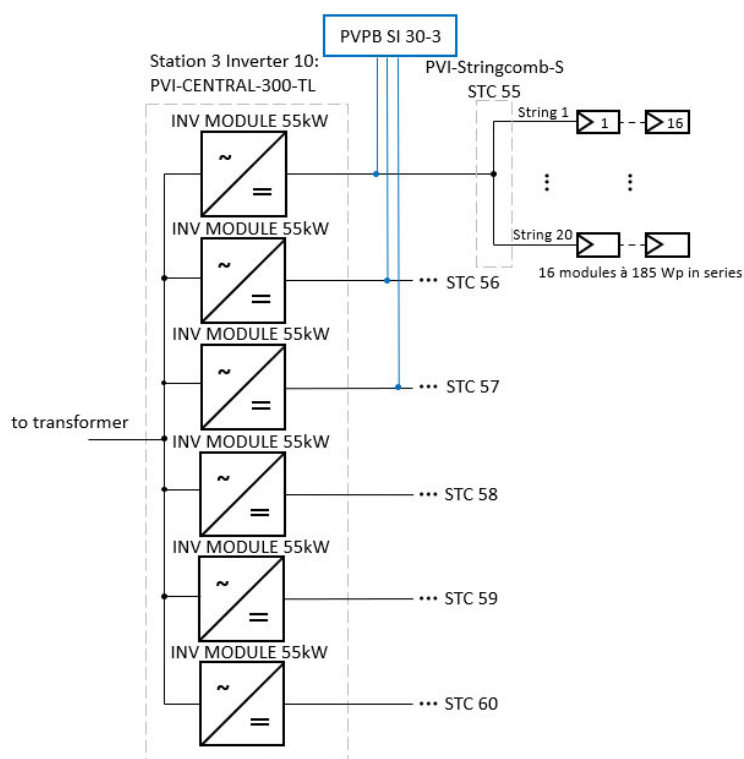


Figure 3-12 schematics of the PVPB installation in the solar park HAI (source: own illustration)

### 3.4.4 RICH – Solar Park Miltenberg

The solar park RICH is located in Lower Franconia, Bavaria. A satellite picture of the park can be seen in Figure 3-13. The park is located between several agricultural fields, and some small shrubbery surrounds it. The topological environment is primarily flat. Another solar park borders the western side, but it is not part of the analysis.





Figure 3-13 Solar Park RICH satellite picture [38]

The nominal power output sums up to 5,721.98 kWp. The commissioning date of the solar park is 23.12.2010, which results in a feed-in tariff of 0.2843 €/kWh. There are five central inverter stations, each containing an inverter of the type ‘REFUSol 630K’. The installed modules consist of 25,410 ‘REC210W – 230W’ modules made of polycrystalline silicon. The general information can be seen in Table 3-4.

Table 3-4 General information about the Solar Park RICH

Solar Park RICH	
Nominal DC power	5,721.98 kWp
Commissioning date	23.12.2010
Modul type	Polycrystalline
Modules	25,410x REC210W – 230W
Inverter concept	Central inverter
Inverters	REFUSol 630K
Feed-in tariff	0.2843 €/kWh

The measurement for the characteristic curve was carried out on 23.06.2020, and the commissioning date of the park is 23.10.2010. The module manufacturer gave a fixed performance guarantee of 90% for the first ten years and 80% for the first 25 years, see Appendix A3-4-1/2/3. Accordingly, the modules must still have an output of above 90% in 2020 and may therefore be a maximum of 10% below their stated rated output. During the characteristic curve measurement, it was noticed that none of the 241 measured strings

performed worse than the maximum allowed -10% by the performance guarantee. Therefore, it can be assumed that the solar park is not affected by PID.

For testing, the PVPB was installed on inverters 2.3 and 2.4, which are located in a common station. The general installation layout can be seen in Figure 3-14. Each of the inverters is connected to its own part of the module array. Therefore, the PVPB must be connected separately to both module arrays.

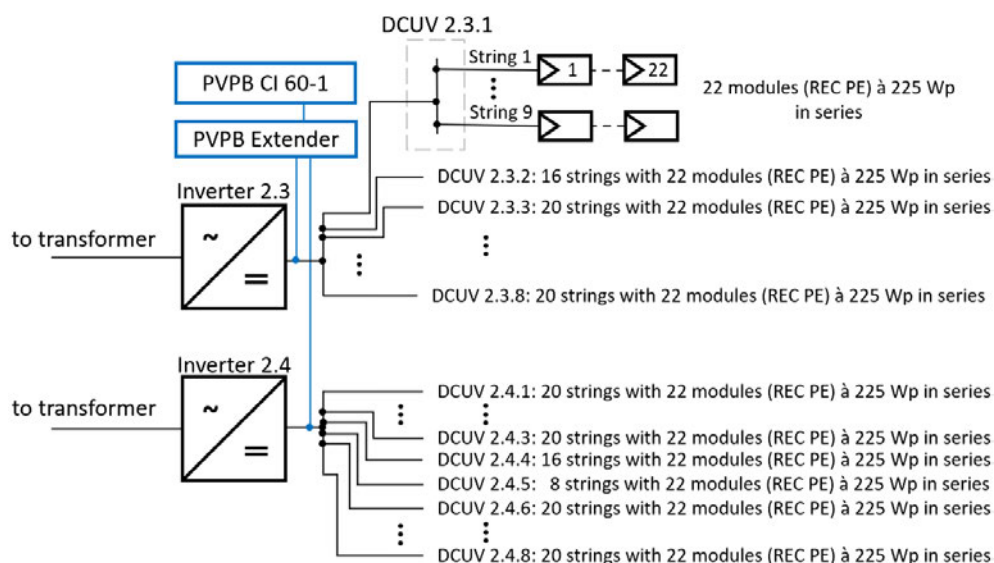


Figure 3-14 schematics of the PVPB installation in the solar park RICH (source: own illustration)

### 3.4.5 KAL – Solar Park Saxony-Anhalt North

The solar park KAL is unique because it has not been equipped with a PVPB, and there are no plans to do so in the future. The park is located in the north of Saxony-Anhalt and has a rated power of 3,651.48 kWp. The module type is polycrystalline. The most important information about the park are listed in Table 3-5.

Table 3-5 General information about the Solar Park KAL

Solar Park Saxony-Anhalt North	
Nominal DC power	3,651.48 kWp
Commissioning date	26.06.2013
Modul type	Polycrystalline
Modules	15,024 CSUN 245-60P
Inverter concept	Central inverter
Inverters	ABB ULTRA-1400.0-TL-OUTD-690
Feed-in tariff	0.1063 €/kWh

In the past, shortly after the completion of the solar park, there were investigations by the operator. These investigations found that the modules were very susceptible to PID, which resulted in the recommendation to ground the park at the minus pole, which was then done. Since this negative-side grounding still exists and it has prevented the PID effect, it should not be removed, and a PVPB box should not be installed.

### 3.4.6 HAL – Solar Park Saxony-Anhalt West

The Solar Park HAL is in the West of the German federal state Saxony-Anhalt and is surrounded by a field on the southern and eastern sides, while it is adjacent to buildings on the western side. The northern part borders a forest. The park is located on a slope with the peak of the slope in the north of the park. In Figure 3-15, a satellite image of the park can be seen.



*Figure 3-15 Solar Park HAL satellite picture*

The nominal capacity of the solar park is 18,193.92 kWp, and it was commissioned on 11.03.2013. The feed-in tariff according to the EEG is therefore 0.1595 €/kWh. The park consists of ten transformer stations. The used inverters are of the type 'SMA SC-800 CP-10' and 'SMA SC-630 CP-10'. These SMA inverters are free-standing units that do not require a station building. The installed modules consist of 75,808 BYD 240 P6-30, which are made of polycrystalline silicon. The essential data is listed in Table 3-6.

## Materials and Methods

Table 3-6 General information about the Solar Park HAL

Solar Park HAL	
Nominal DC power	18,193.92 kWp
Commissioning date	11.03.2013
Modul type	Polycrystalline
Modules	75,808x BYD 240 P6-30
Inverter concept	Central inverter
Inverters	14x SMA SC-800 CP-10 4x SMA SC-630 CP-10
Feed-in tariff	0.1595 €/kWh

No characteristic curve measurement was carried out for the Solar Park HAL. Therefore, no statement can be made about the degree of degradation of the modules.

The WPW23 GU100 inverter was selected to test the PVPB. The PVPB is connected to the DC busbar of the inverter and thus connected to the entire module array. The general layout of the inverter and the PVPB is shown in Figure 3-16.

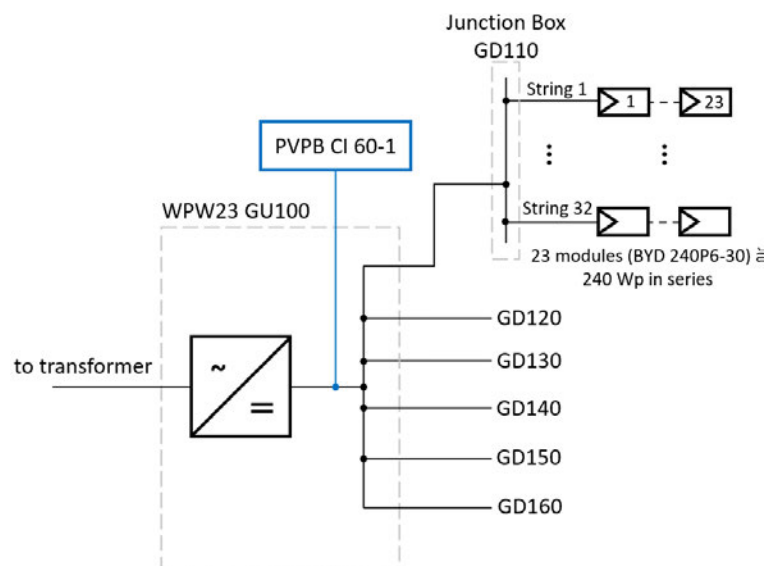


Figure 3-16 schematics of the PVPB installation in the solar park HAL (source: own illustration)

### 3.4.7 FREI – Solar Park Mannheim

The solar park FREI is located in the German state of Rhineland-Palatinate. The park is located alongside a railroad line and therefore has a non-exact orientation to the south. In the first south-western part, the park has an orientation of 14° to the east, and in the second north-

eastern part an orientation of 20° to the east. The railroad line runs along the south side of the park. Agricultural fields surround the other sides. Topologically, the park is located on one level. In Figure 3-17 the satellite image of the park can be seen.



Figure 3-17 Solar Park FREI satellite picture [38]

The nominal capacity of the solar park is 7,302.96 kWp, and it was commissioned on 29.06.2013. The feed-in tariff, according to the EEG, is therefore 0.1063 €/kWh. The park consists of four transformer stations. The used inverters are of the type ‘SMA SC-800 CP-10’ and ‘SMA SC-630 CP-10’. These SMA inverters are free-standing units, which do not require a station building. The installed modules consist of 29,808 CanadianSolar CS6P 245P, which are made of polycrystalline silicon. The essential data is listed in Table 3-7.

Table 3-7 General information about the Solar Park FREI

Solar Park FREI	
Nominal DC power	7,302.96 kWp
Commissioning date	29.06.2013
Modul type	Polycrystalline
Modules	29,808x CanadianSolar CS6P 245P
Inverter concept	Central inverter
Inverters	6x SMA SC-800 CP-10 2x SMA SC-630 CP-10
Feed-in tariff	0.1063 €/kWh

The measurement of the characteristic curve was carried out on 21.08.2019. The commissioning date of the park is 29.06.2013. The module manufacturer gave a linear

performance guarantee starting from 97% in the first year to 90% in the tenth year until 80% in the 25th year, see Appendix A3-7-1. Accordingly, the modules must still have an output of 92.8% in 2019 and may therefore be a maximum of 7.2% below their stated rated output. During the characteristic curve measurement, it was noticed that 57 of 153 measured strings performed worse than the maximum allowed -7.2% by the performance guarantee.

The WPW12 GU200 was selected as the reference inverter. The PVPB was attached to it and connected to the DC busbars of the inverter. The general layout and connection of the PVPB is shown in Figure 3-18.

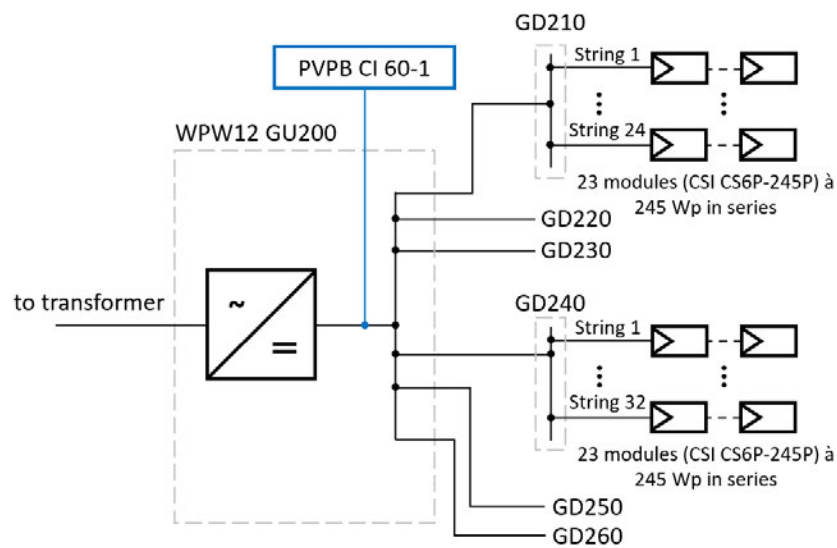


Figure 3-18 schematics of the PVPB installation in the solar park FREI (source: own illustration)

### 3.4.8 EGG – Solar Park Berlin East

The solar park EGG is located in the German state of Brandenburg and borders a forest on its northern side. Along the other sides of the park are open field areas. Topologically, the park is located on a flat plane. In Figure 3-19 the satellite image of the park can be seen.





Figure 3-19 Solar Park EGG satellite picture [38]

The nominal capacity of the solar park is 20,032.32 kWp, and it was commissioned on 26.09.2012. According to the EEG, the feed-in tariff is therefore 0.1595 €/kWh. The park consists of eleven transformer stations. The used inverters are of the type ‘SMA SC-800 CP-10’ and ‘SMA SC-630 CP-10’. These SMA inverters are free-standing units that do not require a station building. The installed modules consist of 16,896 CanadianSolar CS6P 225P and 66,924 Canadian Solar CS6P 240P, which are made of polycrystalline silicon. The essential data is listed in Table 3-8.

Table 3-8 General information about the Solar Park EGG

Solar Park Berlin East	
Nominal DC power	20,032.32 kWp
Commissioning date	26.09.2012
Modul type	Polycrystalline
Modules	16,896x CanadianSolar CS6P 235P 66,924x CanadianSolar CS6P 240P
Inverter concept	Central inverter
Inverters	17x SMA SC-800 CP-10 4x SMA SC-630 CP-10
Feed-in tariff	0.1595 €/kWh

No characteristic curve measurement was carried out for the Solar Park EGG. Therefore, no statement can be made about the degree of degradation of the modules.

The inverter 'WPW14 GU100' was selected as the test inverter. The PVPB box was connected to the DC busbar directly in front of the inverter. The general layout and connection of the PVPB is shown in Figure 3-20.

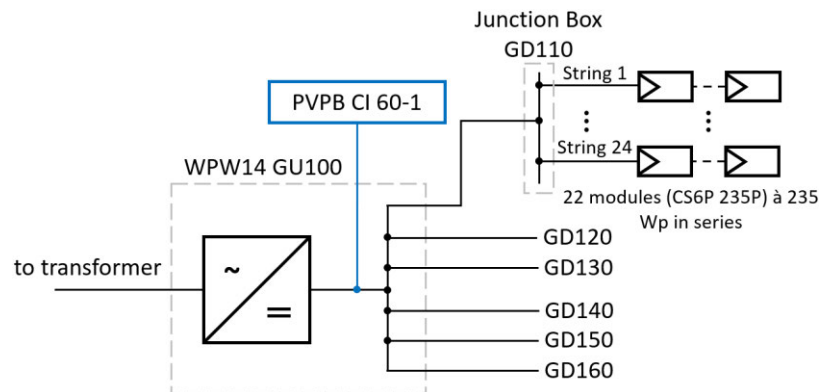


Figure 3-20 schematics of the PVPB installation in the solar park EGG (source: own illustration)

### 3.4.9 AHL – Solar Park Bremen

The solar park AHL is located near Bremen and was built around an airfield. The solar park is divided into five project companies. Three of them are located above the runway and two below it. For the PVPB box investigation, each solar park was considered in its own right, and each one was equipped with a PVPB box. For this reason, each park must be considered separately. The terrain around the solar park is very diverse. To the south there are several hangers and free areas. To the west and east are open areas. To the north are small wooded areas and residential areas. Between the different parts of the park is the runway of the former airfield. The terrain is flat and level. Figure 3-21 shows the satellite image of the park in which only the entire solar park is outlined in red. There is no subdivision into the individual park sections.



Figure 3-21 Solar Park AHL satellite picture [38]



The nominal capacity of the solar parks in sum is 51,272.24 kWp, and they were commissioned on 28.12.2011 and 25./26.06.2012. According to the EEG, the feed-in tariff is therefore 0.2207 €/kWh and 0.1876 €/kWh. Each park consists of several transformer stations, reaching from 5 to 10, summing up in 27. The used inverters are of the type 'Power-One PVI-330.0-TL', 'Power-One PVI-220.0-TL', and 'voltwerk electronics VIS 1200'. The installed modules consist of CanadianSolar CS6P 235-240P and Sun Earth 60P 235-240W, which are both made of polycrystalline silicon. The essential data of every park is listed in Table 3-9.

Table 3-9 General information about the Solar Park AHL

AHL	AHL1	AHL2	AHL3	AHL4	AHL5
Nominal DC power [kWp]	9,179.16	8,899.92	6,733.64	13,558.56	12,900.96
Commissioning date	28.12.2011		25.06.2012		26.06.2012
Module type	Polycrystalline				
Modules	35,016x CS6P 235P 3,960x CS6P 240P	37,872x CS6P 235P	28,824x CS6P 235P	57,696x Sun Earth-60P 235Wp	18,720x Sun Earth 60P 235Wp 35,424x Sun Earth 60P 240Wp
Inverter concept	Central inverter				
Inverters	24x Power-One PVI-330.0-TL 1x Power-One PVI-220.0-TL	24x Power-One PVI-330.0-TL	5x voltwerk electronics VIS 1200	10x voltwerk electronics VIS 1200	10x voltwerk electronics VIS 1200
Feed-in tariff	0,2207 €	0,2207 €	0,1876 €	0,1876 €	0,1876 €

No characteristic curve measurement was carried out for the Solar Park AHL. For this reason, no statement can be made about the degree of degradation of the modules.

There are two main configurations of how the inverters are layed out in the solar park and how the PVPB boxes can be connected to the inverters. In AHL1 the PVPB is connected to the inverter '01.01'. In AHL2 the PVPB box is connected to inverter '07.04'. The general layout of the wiring and the connection location of the PVPB box for both parks can be seen in Figure 3-22.

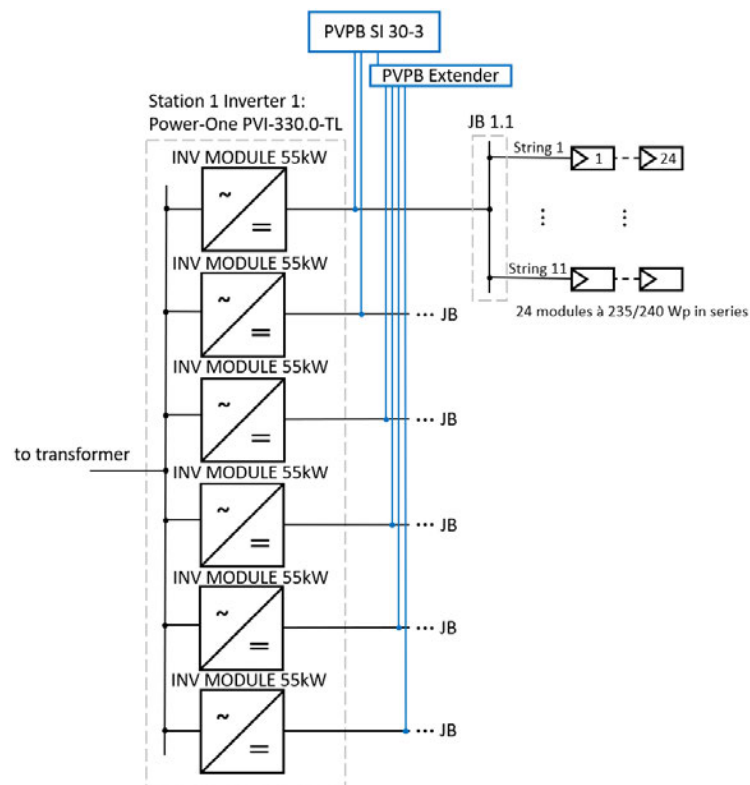


Figure 3-22 schematics of the PVPB installation in the solar park AHL1-2 (source: own illustration)

In AHL3 the PVPB box is connected to inverter '3.3.2', in AHL4 to inverter '4.6.1' and in AHL5 to inverter '5.3.1'. The general layout of the wiring of AHL3-5 can be seen in Figure 3-23.

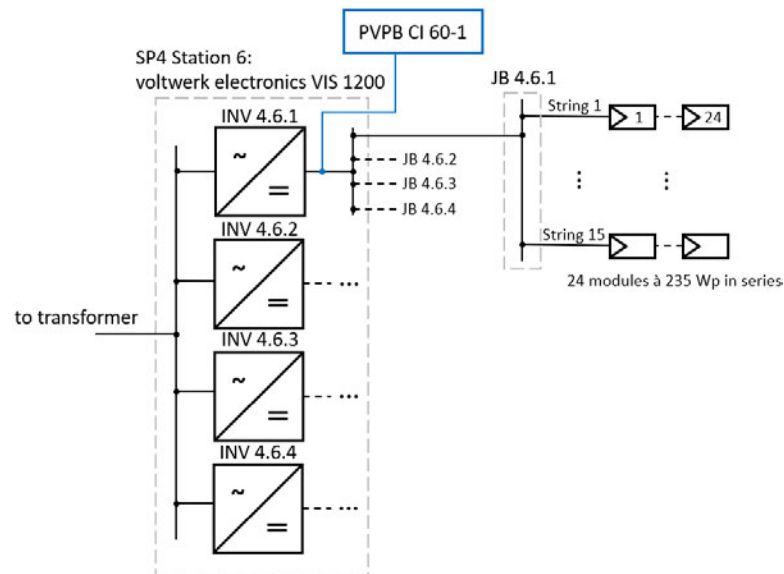


Figure 3-23 schematics of the PVPB installation in the solar park AHL3-5 (source: own illustration)

### 3.4.10 ROHR – Solar Park Thuringia South

The solar park ROHR is located in the south of Thuringia. It is built around a cul-de-sac, and its eastern side borders a commercial area. A green strip borders the south side. Fields border the western and northern sides. The park is located on a slope, with the highest point in the west and the lowest point in the east. Figure 3-24 shows the satellite image of the park.



Figure 3-24 Solar Park Thuringia South satellite picture [38]

The nominal capacity of the solar park is 4,696.80 kWp, and it was commissioned in two steps on 26.09.2011 and 08.03.2012. The two-part commissioning date also causes two different feed-in tariffs. The feed-in tariff, according to the EEG, is therefore 0.2110 and 0.1794 €/kWh.

The park consists of two inverter stations. The used inverters are of the type 'Siemens SINVERT 2200 MS'. The installed modules consist of 24,720 Sunowe SF 190, which are made of monocrystalline silicon. The essential data is listed in Table 3-10.

*Table 3-10 General information about the Solar Park ROHR*

Solar Park ROHR	
Nominal DC power	4,696.80 kWp
Commissioning date	I: 29.12.2011 II: 08.03.2012
Modul type	Monocrystalline
Modules	24,720 Sunowe SF 190
Inverter concept	Central inverter
Inverters	2x Siemens SINVERT 2200 MS
Feed-in tariff	I: 0.2110 €/kWh II: 0.1794 €/kWh

No characteristic curve measurement was carried out for the Solar Park ROHR. For this reason, no statement can be made about the degree of degradation of the modules.

Inverter station one was selected as the test inverter. The PVPB box was connected to the DC busbar directly in front of the inverter. The general layout and connection of the PVPB is shown in Figure 3-25.

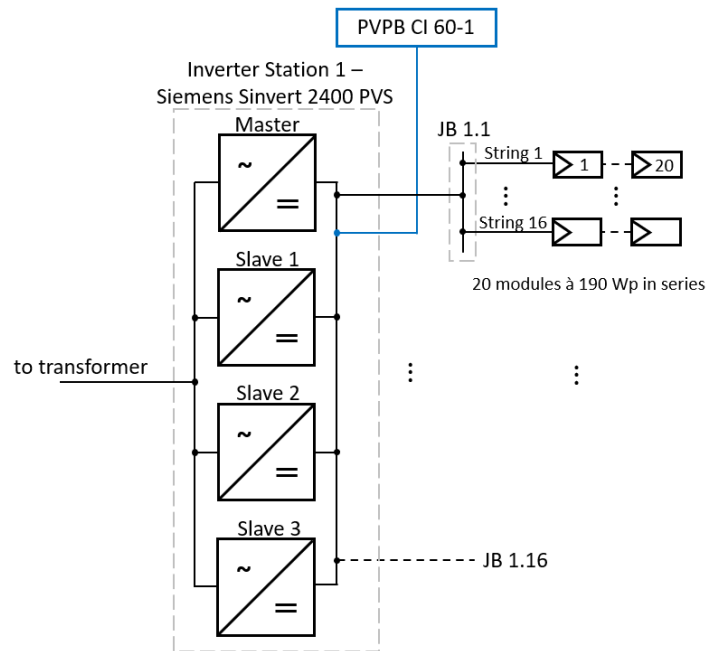


Figure 3-25 schematics of the PVPB installation in the solar park ROHR (source: own illustration)

### 3.4.11 ELS – Solar Park Saxony East

The ELS solar park is located in the east of Saxony and is surrounded by forest on all its sides. Topologically, the terrain is mainly flat. Figure 3-26 shows the satellite image of the park.



Figure 3-26 Solar Park ELS satellite picture [38]

The nominal capacity of the solar park is 20,004.4 kWp, and it was commissioned on 23.12.2011. According to the EEG, the feed-in tariff is therefore 0.2207 €/kWh. The park consists of 18 inverter stations. The used inverters are of the type ‘Solarmax Sputnik Engineering 990TS-SV Single MPP’. The installed modules consist of 560x Sunowe 225-M, 24,640x Sunowe 225-P, 33,039x Sunowe 230-P, and 27,998x Sunowe 235-P, which are made of polycrystalline silicon. The essential data is listed in Table 3-11.

*Table 3-11 General information about the Solar Park ELS*

Solar Park ELS	
Nominal DC power	20,004.4 kWp
Commissioning date	23.12.2011
Modul type	Polycrystalline
Modules	560x Sunowe 225-M 24,640x Sunowe 225-P 33,039x Sunowe 230-P 27,998x Sunowe 235-P
Inverter concept	Central inverter
Inverters	18x Solarmax Sputnik Engineering 990TS-SV Single MPP
Feed-in tariff	0.2207 €/kWh

The measurement for the characteristic curve was carried out on 31.07.2019. The commissioning date of the park is 23.12.2011. The module manufacturer gave a fixed performance guarantee of 90% for the first ten years and 80% for the first 25 years, see Appendix A3-11-1. Accordingly, the modules must still have an output of above 90% in 2019 and may therefore be a maximum of 10% below their stated rated output. With linear regression, on the other hand, the modules should have an output of 92% in 2019 and may therefore be a maximum of 8% below their stated rated output. During the characteristic curve measurement, it was noticed that five of the 60 measured strings performed worse than the theoretical maximum allowed -8% by the linearly viewed performance guarantee.

For testing, the PVPB was installed in inverter station 14. The general installation layout can be seen in Figure 3-27. There are three 'SM330TS-SV' inverters from the manufacturer 'Solarmax' in one inverter station. Each of the three inverters consists of three smaller sub-units. However, all inverters in a station are connected to the module field via a common busbar, which means that the PVPB box can be connected to this busbar.

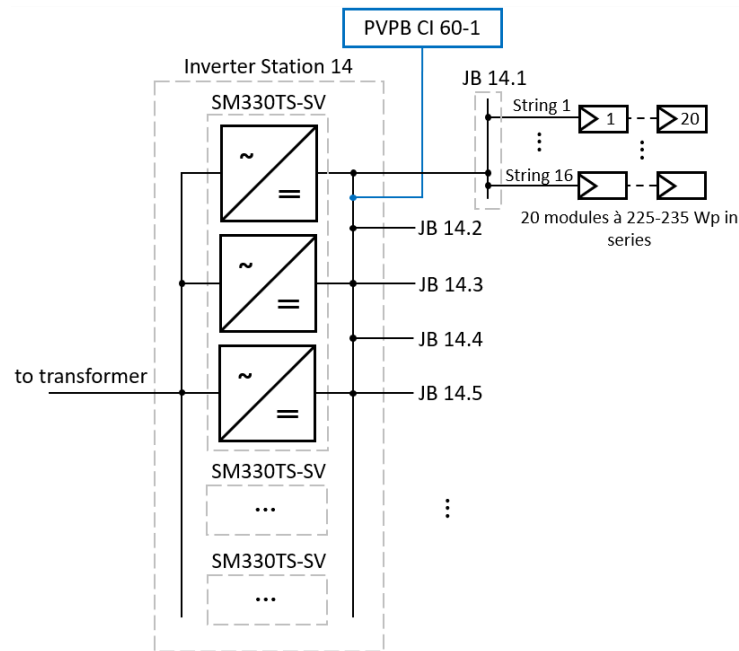


Figure 3-27 schematics of the PVPB installation in the solar park ELS (source: own illustration)

### 3.5 Cost Breakdown

The costs for purchasing and installing the PV Booster Box are considered broken down per solar park. Each solar farm is represented in a separate special purpose vehicle, a subsidiary of the parent company, which owns all the solar parks under investigation.

In Table 3-12 the costs for all the solar parks are listed. The total price consists of the purchase price of the PVPB, the installation costs, and the auxiliary material, which is already included in the installation costs. A coordination fee is added for each material or service purchased externally, which does not originate from the operating company itself. Consequently, the PV Booster Box price is composed of the box, the associated fuses, the configuration, the freight costs, and the coordination fee. Installation costs include labor, auxiliary materials, travel time, and any overnight accommodations. A coordination fee on materials and on services will be charged for work performed by outside contractors. It should be noted that all prices are given in their net amounts. The value-added tax is not considered at any time.

Table 3-12 Overview of PVPB & installation costs

Park	PVPB Box	Installation Costs	Yield loss	Total costs
EHEU	6.882,94 €	1.829,90 €	1.343,19 €	10.056,03 €
FOR	439,88 €	233,60 €	42,37 €	715,85 €
HAI	1.165,83 €	1.391,30 €	91,97 €	2.649,09 €
RICH	1.641,35 €	547,36 €	248,23 €	2.436,94 €
HAL	1.482,86 €	1.210,80 €	0,00 €	2.693,66 €
FREI	1.482,86 €	1.068,00 €	7,17 €	2.558,03 €
EGG	1.513,13 €	593,70 €	54,28 €	2.161,11 €
AHL1	1.288,46 €	1.044,50 €	182,91 €	2.515,86 €
AHL2	1.288,46 €	922,10 €	0,00 €	2.210,56 €
AHL3	1.634,44 €	1.113,19 €	35,25 €	2.782,89 €
AHL4	1.634,44 €	1.332,24 €	11,11 €	2.977,80 €
AHL5	1.667,80 €	1.113,19 €	32,76 €	2.813,75 €
ROHR	1.667,80 €	1.406,60 €	39,23 €	3.113,63 €
ELS	1.513,13 €	1.751,40 €	10,11 €	3.274,64 €

In addition to the costs, there are the yield losses incurred during the installation of the PVPB box. While these are not costs that must be paid, they are lost revenues that the solar farm would otherwise have earned. Therefore, the yield losses are included here to represent the actual cost of installing the PVPB boxes. The yield losses are calculated based on the specific yield values on the day of installation. First, the mean value of the specific yield of the reference area without a PVPB box is calculated ( $Y_{ref.area}$ ), from which the specific yield value of the inverter with an installed PVPB box is subtracted ( $Y_{inv\ with\ PVPB}$ ). The resulting specific yield value is multiplied by the nominal power of the inverter to which the PVPB box was attached ( $P_{STC,inv\ with\ PVPB}$ ). The calculation of the yield loss ( $W_{yield\ loss}$ ) in kWh can be seen in Formula 3.2.

$$W_{yield\ loss} = (Y_{ref.area} - Y_{inv\ with\ PVPB}) * P_{STC,inv\ with\ PVPB} \quad (3.2)$$

Nevertheless, when installing the PVPB boxes, care was taken to minimize yield losses by preparing the work in the afternoon and only turning off the inverters for installation in the evening. However, this still resulted in a slight yield loss in some cases.



It should be stated that the installation costs are primarily made up of travel costs, as there have been some very long journeys. These can be reduced by good planning in combination with other operations taking place simultaneously.

### 3.6 Analysis Method

To evaluate the results, the historical inverter yield data for the period since the installation of the PVPB are downloaded from the technical operator's respective monitoring portal. The used inverter data are specific yield values composed of the energy yield and the connected DC nominal power of the inverter. If no specific values were available, the specific yield values were calculated using Formula 3.3 [8].

$$Y_F = \frac{W_{AC}}{P_{STC}} * \frac{kWh}{kWp} \quad (3.3)$$

The specific yield was used to make all inverter values comparable since the inverters can have different DC-nominal power and therefore different energy yields. The values were compared on a daily basis since the installation of the PVPB box until 31.01.2022. To determine an improvement in yield due to the installation of the PVPB box, the mean value of the inverters equipped with a PVPB box was set in relation to the inverters without a PVPB box installed. The area with the inverters without a PVPB box is defined as the reference area. In order to be able to draw a trend, the specific yield value of the reference area is divided by the specific yield value of the inverters with a PVPB box, as seen in Formula 3.4.

$$ratio [\%] = \frac{Y_{inv \text{ with PVPB box}}}{Y_{reference \text{ area}}} * \frac{\frac{kWh}{kWp}}{\frac{kWh}{kWp}} \quad (3.4)$$

The ratio of the two values can be used to determine a trend by linear regression. The linear regression calculates by how many percent the specific yield has increased due to the installation of a PVPB box.

It is essential that failures of the inverters or other yield-related components are taken into account, as they could otherwise distort the result. The failures and downtimes of a solar park are tracked by the technical operator. For this purpose, the technical operator of each solar park prepares a monthly report listing all incidents in the solar park. These reports have been analyzed for each solar park since the installation of the PVPB box, and all outages with yield

losses have been calculated out in the analysis of the results. This was realized by ignoring the affected devices as a value on the affected days.

In addition, it has happened that not all incidents were listed in the reports of the technical operators. During the analysis of the results, zero values were automatically excluded, as they would additionally distort the result.

As a further means of removing further inaccuracies from the comparison, days on which snow was present were removed entirely from the calculation of the linear trend. For this purpose, the images of the cameras available in the park were evaluated for each solar park on each day of the analysis and checked for snowfall. In each solar park studied, a camera regularly takes pictures of the module tables to enable the technical operator to check for snowfall. So if there is snow on the modules, it can happen that it slides down or melts faster in some areas than in others. Thus, the areas of the solar farm can produce more energy where the snow disappears faster. For this reason, days when the modules are covered with snow have been wholly excluded from the calculation.

In order to determine that the possible calculated improvement due to the installation of the PVPB box is not a recurring annual effect, the additional yield value must be compared with the previous year. To do this, the same analysis is performed with a review of technical reports and snow days for the same period with the same reference range a year earlier. This determined gain value from the previous year ( $G_{2020/21 \text{ without PVPB}}$ ) is subtracted from the gain value from the current year ( $G_{2021/22 \text{ with PVPB}}$ ) to obtain a realistic estimate of the actual additional yield ( $G_{real}$ ) as it can be seen in Formula 3.5.

$$G_{real} = G_{2021/22 \text{ with PVPB}} - G_{2020/21 \text{ without PVPB}} \quad (3.5)$$

### 3.7 Dedicated Voltage Measurement in AHL

Within the scope of the thesis, a field measurement was carried out to verify the PVPB box's function and show a possible increase of the MPP voltage by reversing the PID effect. Therefore a voltage measurement was installed in the solar park AHL, which measures the voltage of the connected junction boxes to the inverter. The measuring device used for this purpose is the 'UT161B' from the company 'UNI-T' [39]. The 'UT161B' is a standard commercially available multimeter that can connect to a PC via USB cable and store its measured values. For this purpose, the software belonging to the multimeter must be installed

on a PC. In the software, the time interval can be set in which the measured values are recorded. For example, every second, every minute, or every hour. The measured values are instantaneous values and have not been averaged or summed.

A total of four multimeters were used for the measurement in AHL, as four readings were to be recorded since the multimeters can only take one reading at a time. To prove the function of the PVPB box, the voltage from the negative pole to ground and from the positive pole to ground of a JB connected to a PVPB box was measured. For this purpose, JB 1.1.1 was used, which is connected to inverter 1.1.1. In order to determine an improvement by reversing the PID effect, the voltage of a JB, which is not connected to a PVPB box, is also measured. The JB 1.1.2.1 was used for this purpose. Again, the voltage from the negative pole to ground and from the positive pole to ground is measured.



*Figure 3-28 Installation of the dedicated voltage measurement*

The four multimeters were installed on 09.11.2021 and operated until 07.02.2022. The setup of the measuring equipment can be seen in Figure 3-28. To prevent the multimeters from shutting down over such a long period of time, the batteries were removed and replaced with an external power supply. The time interval for the measurement was selected to be one value per minute.

First of all, the voltage measurements are meant to show and prove the functionality of the PVPB boxes. It should also demonstrate how the PVPB box switches on and off and which voltage it applies to the module field at night.

Secondly, the reversal of the PID effect by the PVPB boxes is attempted to be shown using the values of the measured string voltage since the PID effect significantly influences the voltage

of the modules. The voltage of the strings depends logarithmically on the irradiation and in combination with a temperature coefficient on the temperature, see Formula 3.6. Therefore, it is essential to consider the irradiance and temperature when investigating whether the reversal of the PID effect can be seen in an increased string voltage. The irradiation and temperature data is provided by a dedicated sensor station located in the park. The sensor station is equipped with two horizontally oriented pyranometers and two inclined irradiance sensors. At the same time, the temperature of the modules is measured at the inclined irradiance sensor since its containing a reference cell. For the evaluation, the irradiance data from the inclined plane is used because it represents the irradiance seen by the modules since the sensors have the same inclination as the modules with 20°. The average value of both irradiation sensors is used. The irradiation and temperature data are only available for each quarter-hour. The irradiation is summed up in the quarter-hour, and the temperature is averaged for the quarter-hour. For this reason, the measured voltage values are also averaged for each quarter-hour.

$$V_{MPP} = V_{MPP0} * \frac{\ln(E)}{\ln(E_{1000})} * (1 + \alpha_U * (\alpha - \alpha_{25})) \quad (3.6)$$

Formula 3.6 is used to calculate the theoretical MPP-Voltage, which the strings should have due to irradiance and temperature, whereby  $V_{MPP0}$  is the specified MPP voltage in the datasheet.  $E$  indicates the current irradiation in  $W/m^2$ .  $\alpha_U$  represents the temperature coefficient, which is specified in the module's datasheet.  $\alpha$  represents the current temperature.  $E_{1000}$  and  $\alpha_{25}$  are constants and shall be  $1000 W/m^2$  and  $25^\circ C$ .

The nominal string voltage  $V_{MPP0}$  of the existing module array is 717.6 V for 24 CS6P 240P modules connected in series. The module's temperature coefficient  $\alpha_U$  for the voltage is  $-0.34 \%/^\circ C$ .

## 4. Results

In the following chapter, the results of the study are presented and graphically depicted. In addition, the field measurement carried out specifically for this purpose is evaluated, and a brief economic evaluation follows at the end.

### 4.1 Yield Gain

The results were determined according to the presented analysis methodology from Chapter 3.6 with Formula 3.4. The data, analysis, and results can be found in Appendix A4-1-1 until A4-1-11.

The evaluation results for the solar park EHEU are shown in Figure 4-1. It can be seen that the inverter equipped with a PVPB had improved compared to the previous year when no PVPB was equipped. The currently determining possible additional yield due to Formula 3.5 is 0.66%.

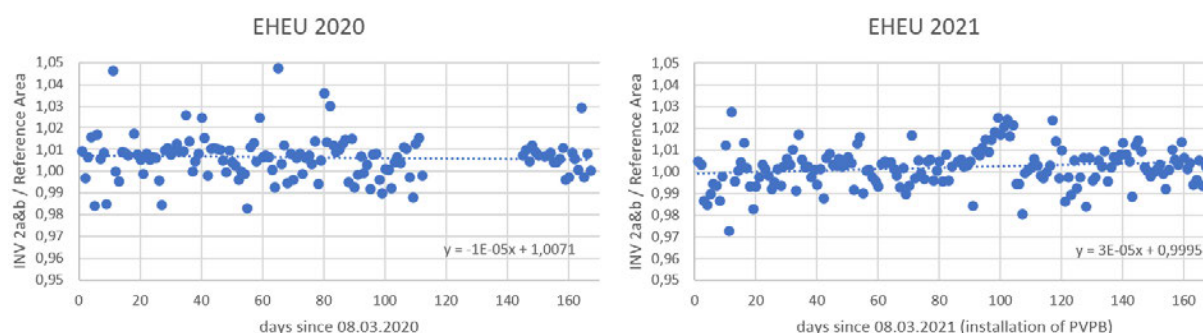


Figure 4-1 EHEU results (right: period with PVPB installed; left: same period one year earlier)

The evaluation results for the solar park FOR are shown in Figure 4-2. It can be seen that the behavior of the inverter equipped with PVPB in the present is similar to the development of the previous year. The currently determined possible additional yield is -0.60% and thus does not represent an improvement in the yield.

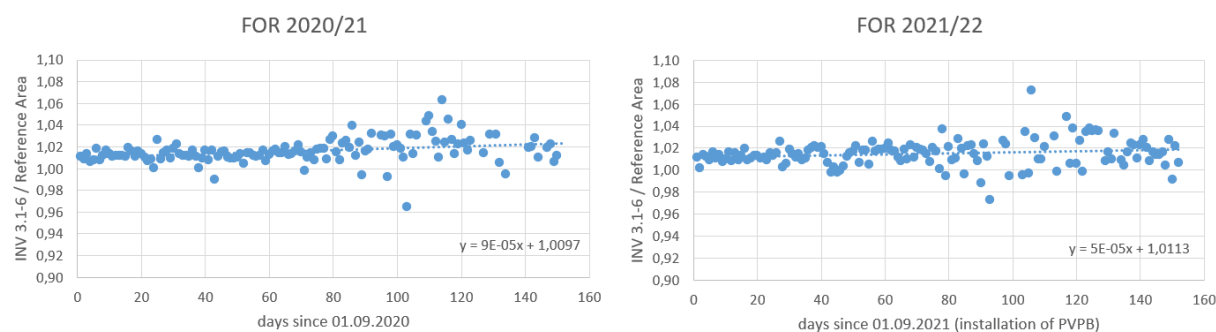


Figure 4-2 FOR results (right: period with PVPB installed; left: same period one year earlier)

## Results

The evaluation results for the solar park HAI are shown in Figure 4-3. It can be seen that the behavior of the inverter equipped with PVPB in the present is similar to the development of the previous year. In both cases, the ratio decreases. The currently determined possible additional yield is -1.58% and therefore does not represent an improvement in the yield.

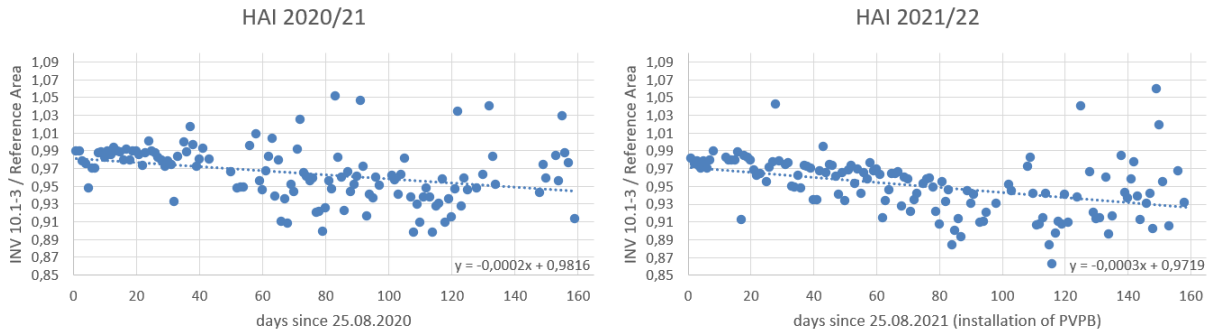


Figure 4-3 HAI results (right: period with PVPB installed; left: same period one year earlier)

The evaluation results for the solar park RICH are shown in Figure 4-4. It can be seen that the behavior of the inverter equipped with PVPB is staying constant in the present, in contrast to the decreasing development in the previous year. The currently determined possible additional yield is 2.49% and therefore does represent an improvement in the yield.

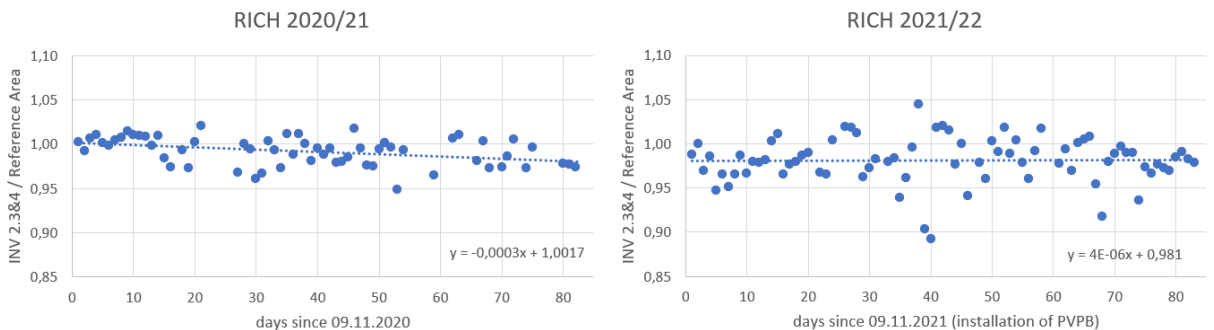


Figure 4-4 RICH results (right: period with PVPB installed; left: same period one year earlier)

The evaluation results for the solar park HAL are shown in Figure 4-5. It can be seen that the behavior of the inverter equipped with PVPB in the present is similar to that in the previous year. Both developments show positive growth. The currently determined possible additional yield is 0.00% and therefore does not represent an improvement in yield.

## Results

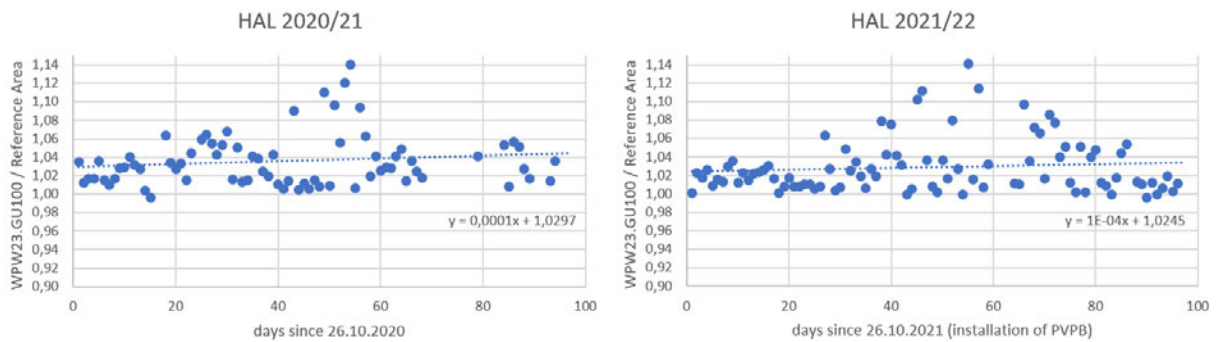


Figure 4-5 HAL results (right: period with PVPB installed; left: same period one year earlier)

The evaluation results for the solar park FREI are shown in Figure 4-6. It can be seen that the behavior of the inverter equipped with PVPB has a negative development in the present, whereas it was positive in the previous year. The currently determined possible additional yield is -1.15% and therefore does not represent an improvement in the yield.

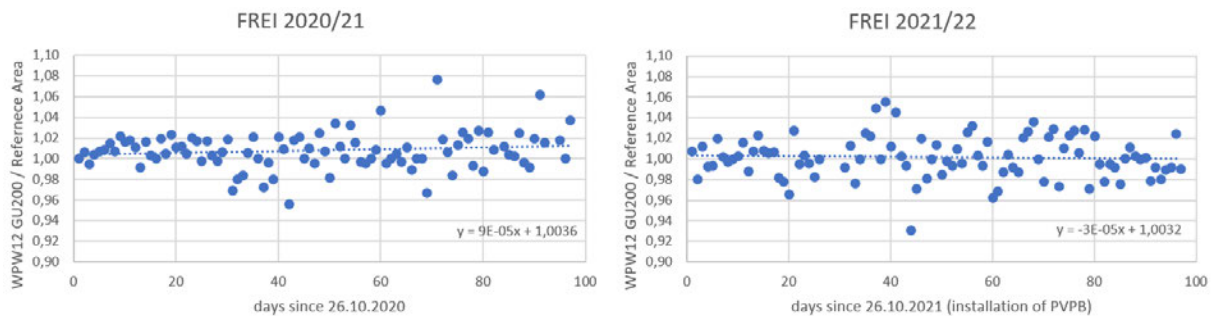


Figure 4-6 FREI results (right: period with PVPB installed; left: same period one year earlier)

The evaluation results for the solar park EGG are shown in Figure 4-7. It can be seen that the behavior of the inverter equipped with PVPB records a positive trend in the present, whereas it is negative in the previous year. The currently determined possible additional yield is 1.32% and thus represents an improvement in the yield.

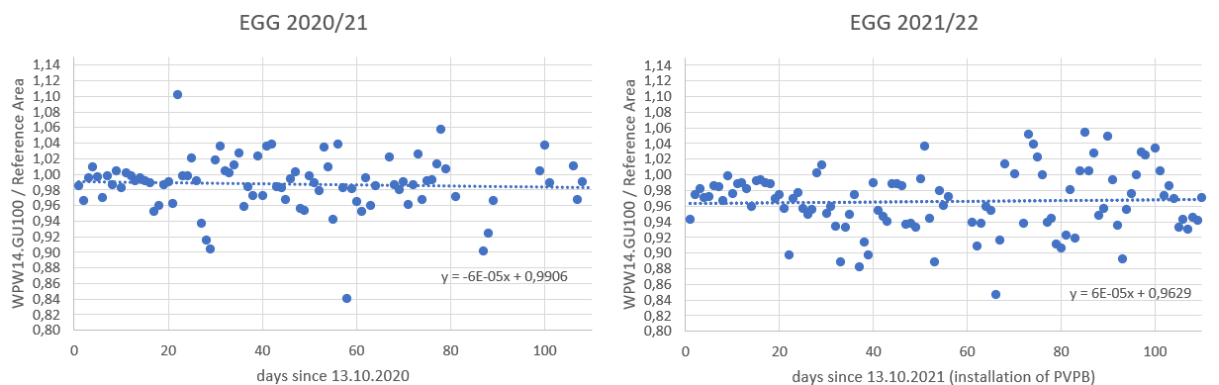


Figure 4-7 EGG results (right: period with PVPB installed; left: same period one year earlier)

## Results

The evaluation results for the solar park AHL1 are shown in Figure 4-8. It can be seen that the behavior of the inverter equipped with PVPB in the present is similar to the previous year without PVPB. The currently determined possible additional yield is 0.82% and thus represents an improvement in the yield.

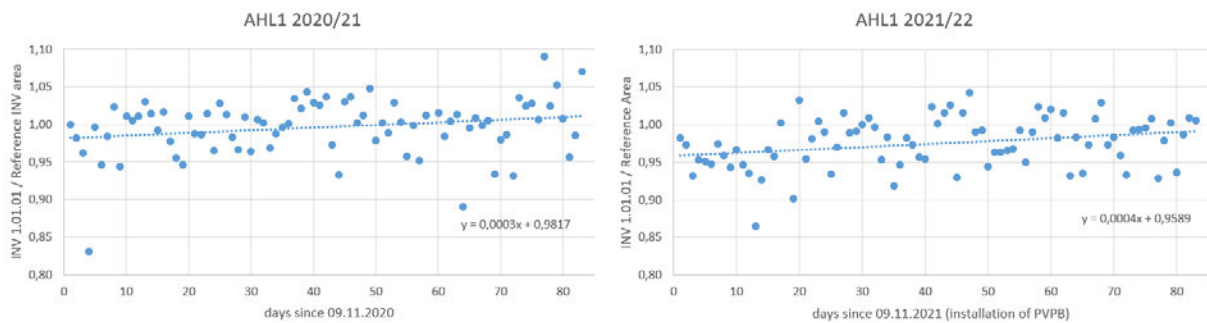


Figure 4-8 AHL1 results (right: period with PVPB installed; left: same period one year earlier)

The evaluation results for the solar park AHL2 are shown in Figure 4-9. It can be seen that the behavior of the inverter equipped with PVPB in the present is similar to the previous year without PVPB. The currently determined possible additional yield is 0.00% and therefore does not represent an improvement in the yield.

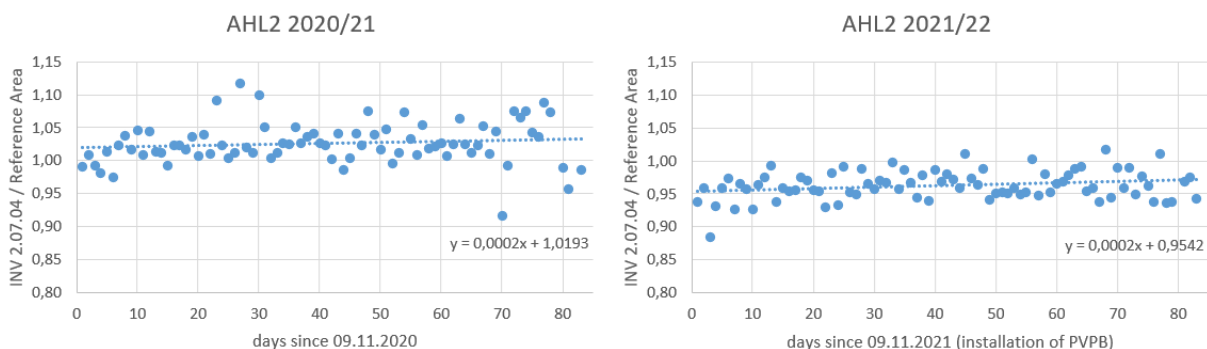


Figure 4-9 AHL2 results (right: period with PVPB installed; left: same period one year earlier)

The evaluation results for the solar park AHL3 are shown in Figure 4-10. It can be seen that the behavior of the inverter equipped with PVPB in the present is similar to the previous year without PVPB. The significantly lower ratio in the current period can probably be attributed to undeclared failures. The currently determined possible additional yield is 1.98% and thus represents an improvement in the yield.



## Results

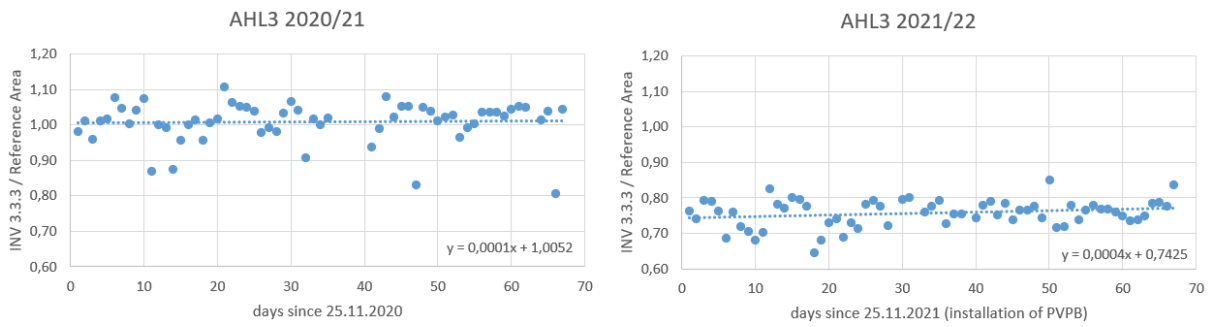


Figure 4-10 AHL3 results (right: period with PVPB installed; left: same period one year earlier)

The evaluation results for the solar park AHL4 are shown in Figure 4-11. It can be seen that the behavior of the inverter equipped with PVPB in the previous year without PVPB differs significantly from the development at the current time with PVPB. A sharp increase in the ratio can be seen in the previous year (2020/21), which is probably due to undeclared failures. The current possible additional yield is -11.88% compared to the previous year. However, since the data from the previous year are not to be reliable, only the development of the current period with 3.30% is used, which again represents a positive effect on the yield.

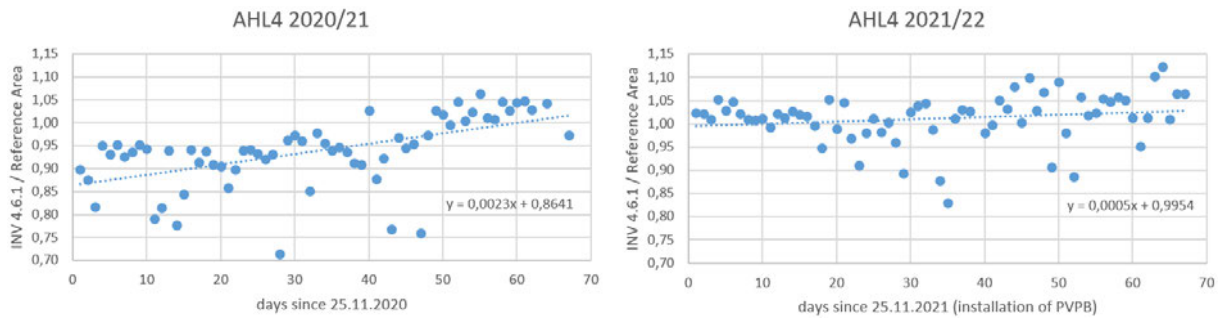


Figure 4-11 AHL4 results (right: period with PVPB installed; left: same period one year earlier)

The evaluation results for the solar park AHL5 are shown in Figure 4-12. It can be seen that the behavior of the inverter equipped with PVPB in the previous year without PVPB differs significantly from the development at the current time with PVPB. A sharp increase in the ratio can be seen in the previous year, which is probably due to undeclared failures. The current possible additional yield is -7.85% compared to the previous year. However, since the data from the previous year is not reliable, only the development of the current period with 0.07% is used, which again represents a positive effect on the yield.

## Results

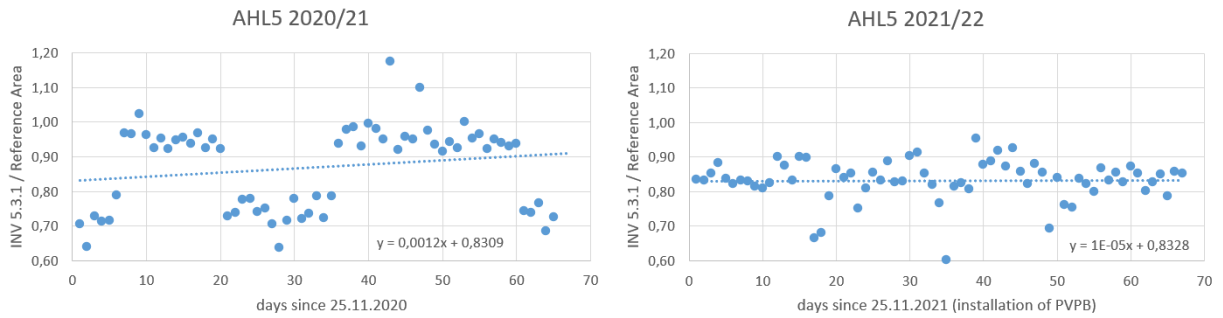


Figure 4-12 AHL5 results (right: period with PVPB installed; left: same period one year earlier)

Figure 4-13 shows the results of the solar park ROHR. The current development in the test year is negative. A comparison with the previous year could not be made, as no data is available for this period. In addition, the evaluation of the current test phase was only carried out until 22.12.2021, as further data is also missing. The development of the current test phase is -2.80% and therefore does not represent an improvement in the yield.

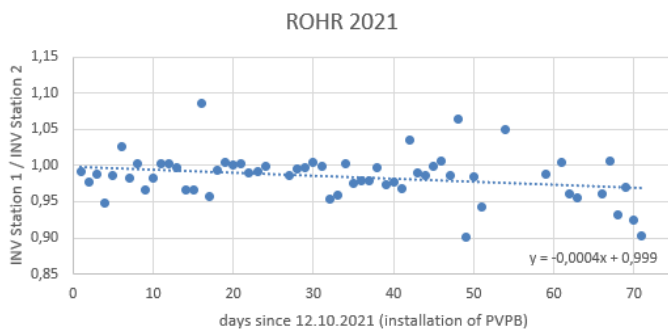


Figure 4-13 ROHR results (period with PVPB installed)

The evaluation results for the solar park ELS are shown in Figure 4-14. It can be seen that the behavior of the inverter equipped with PVPB in the present is positive, whereas the development in the previous year was more positive. The currently determined possible additional yield is -0.71% and therefore does not represent an improvement in the yield.

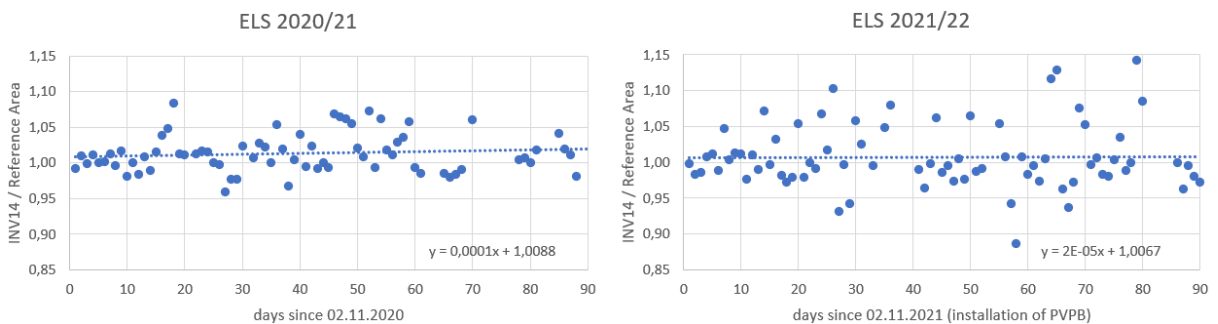


Figure 4-14 ELS results (right: period with PVPB installed; left: same period one year earlier)

## Results

---

The results of the individual solar parks are listed in Table 4-1. The results are very mixed, and there are some adverse developments and some positive developments. It remains to be noted that the very high percentages in AHL4 and AHL5 in the previous year are probably due to failures that were not taken into account. The solar park KAL was not considered here because it was not equipped with a PVPB.

*Table 4-1 Results of all solar parks*

<b>Park</b>	<b>Ratio Yield Gain in 2020/21</b>	<b>Ratio Yield Gain in 2021/22</b>	<b>Gain</b>
EHEU	-0.17 %	0.50 %	0.66 %
FOR	1.36 %	0.75 %	-0.60 %
HAI	-3.16 %	-4.74 %	-1.58 %
RICH	-2.46 %	0.03 %	2.49 %
HAL	0.96 %	0.96 %	0.00 %
FREI	0.86 %	-0.29 %	-1.15 %
EGG	-0.65 %	0.65 %	1.31 %
AHL1	2.46 %	3.28 %	0.82 %
AHL2	1.64 %	1.64 %	0.00 %
AHL3	0.66 %	2.64 %	1.98 %
AHL4	15.18 %	3.30 %	-11.88 %
AHL5	7.92 %	0.07 %	-7.85 %
ROHR	n.a.	-0.71 %	-0.71 %
ELS	0.89 %	0.18 %	-0.71 %

### 4.2 Field Measurements

The voltage measurement has been partially successfully implemented in AHL. All four multimeters were connected to the respective JB voltage and connected to a PC installed on site. The measurement of the JB connected to the PVPB box was successful, and one-minute readings for negative to ground and positive to ground are available. The measurement of the JB, which is not connected to the PVPB box, failed. The PCs that were supposed to take the readings crashed and therefore did not store any data.

The raw data and the corresponding evaluation can be seen in appendix A4-2-1.

Figure 4-15 shows the voltage curve of the JB 1.1.1.1 from 12:00 on 10.11.2021 until 11:59 on 11.11.2021. The measurement includes the voltage of the negative pole to ground (blue) and the positive pole to ground (red), as well as the resulting string voltage (gray). It can be seen that during the operation at daytime, the installed inverter (Power-One PVI-330.0-TL) builds up the string voltage symmetrically around the ground potential of 0V, and the voltage of the positive and negative string pole are equal in magnitude.

The later it gets, the lower the string voltage becomes. From around 17:00, the string voltage drops drastically from over 400V to just over 100V. The string voltage continues to drop until it reaches 33V at 17:24. The switch-on limit of the PVPB box is 30V. The measured value two minutes later at 17:26 already shows that the PVPB box has started to operate. The voltage at the negative and positive poles is already about 440V with respect to ground. However, the PVPB box should be parameterized to 700V with respect to ground and should apply 700V to the negative and positive poles. One reason for the deviation may be incorrect parameterization. Further reasons can be higher than expected earth currents in the module field. The PVPB box applies a voltage to the strings and can supply a maximum output current of 60 mA. However, if the ground current in the connected module array exceeds 60 mA, the PVPB box will continue to supply 60 mA, but the voltage will drop, also called derating. However, in the case of derating, the voltage would vary significantly more and not remain constant, as it is the case here. The cause is probably a wrong parameterization.

The manufacturer of the PVPB boxes has stated that the 400V set is too low to reverse the PID effect. Reversal works best at a minimum of 700V. Nevertheless, the function of the PVPB is also given at only 440V to a minimal extent. However, the reversal of a possible PID effect takes significantly longer or only prevents the progression of a possible PID effect and cannot reverse it.

The next day around 07:00, the string voltage increases due to the rising of the sun. The PVPB box notices this and switches off at a voltage of over 60V caused by the module field, which was the case at 07:09.

## Results

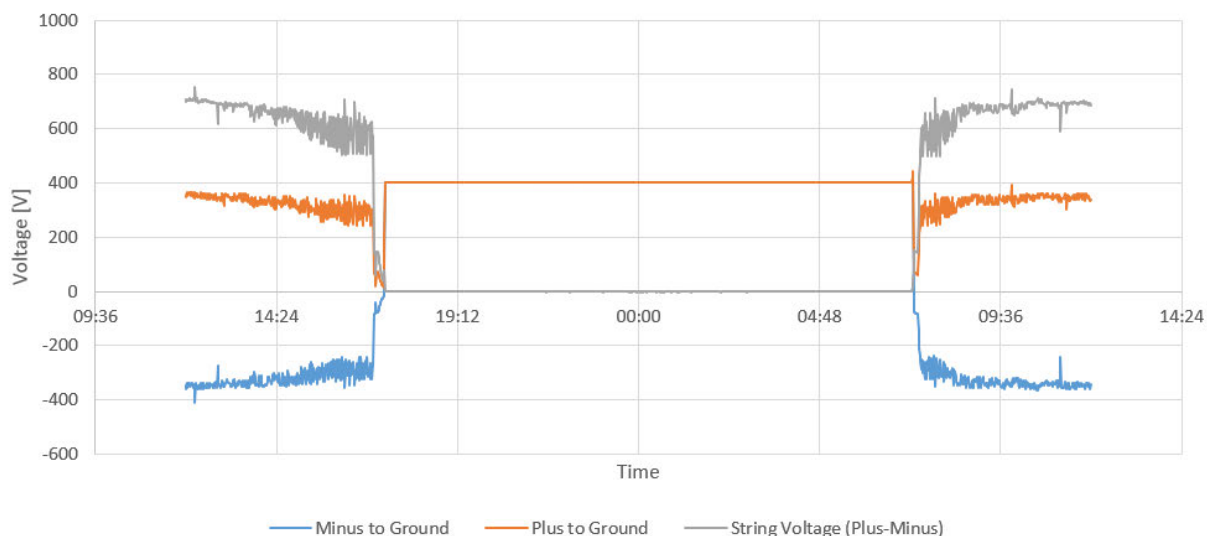


Figure 4-15 Voltage Measurement from 10.11.2021 12:00 until 11.11.2021 11:59 (source: own illustration)

In addition to the functional check of the PVPB box, it should also be evaluated if the PVPB box caused a reversal of a potential PID effect. Since the PID effect affects the voltage primarily, an attempt was made to determine a reversion of the PID effect via a possible increase in the MPP voltage. Since theoretically, if the PVPB box could reverse the PID effect, the actual measured MPP voltage should be more significant compared to the theoretical MPP voltage calculated from irradiance and temperature data. For calculating the theoretical string voltage, Formula 3.4 was used, as mentioned before. Thus, for each quarter of an hour, a value for the theoretical string voltage was calculated using the irradiation in  $\text{W}/\text{m}^2$  and the temperature of the modules in  $^{\circ}\text{C}$ . Then the theoretical string voltage was put in relation to the actual measured string voltage. However, it has been found that the theoretically calculated string voltages deviate significantly from the real measured ones and are similar to the measured values only at high irradiation values.

Table 4-2 shows two exemplary pairs of values of consecutive quarter hours.

The first two values, recorded on 10.11.2021 at 13:00 and at 13:15, demonstrate how much the actual measured and the theoretical string voltage differ. The irradiance is very low with 56 to 68  $\text{W}/\text{m}^2$ . However, the theoretically calculated voltage is about 50% lower than the actually measured voltage.

The other two measured values are from 12.11.2021 13:00, and 13:15. Here the irradiation is more significant and amounts to 537 and 516  $\text{W}/\text{m}^2$ . The theoretically calculated string voltage is now only 2 and 10 % below the actual measured string voltage. However, it is noticeable

that the measured string voltage increases from 13:00 to 13:15, although the irradiation decreases and the temperature increases, which should have the opposite effect.

Various factors can explain this. On the one hand, the sensor station has a certain inaccuracy and records the irradiation data and temperature data with a measurement inaccuracy. In addition, the sensor station is not exactly next to the measured module field and thus represents the irradiation at a location less than a hundred meters away. In the case of changeable cloud cover, the sensor station may record different irradiation in its 15-minute interval than encountered in the corresponding module field.

Table 4-2 Voltage measurement example values

Date	$V_{String}$ [V]	$E$ [W/m <sup>2</sup> ]	$T$ [°C]	$V_{String,theo.}$ [V]	$\frac{V_{String}}{V_{String,theo.}}$
10.11.2021 13:00	686.1	68.1	11.8	458.1	1.498
10.11.2021 13:15	685.1	56.3	11.6	437.8	1.565
12.11.2021 13:00	690.0	536.8	16.7	671.4	1.028
12.11.2021 13:15	723.3	516.3	22.1	655.3	1.104

Data points with good irradiance values have to be compared to draw a trend. It would be best if the data points have the same conditions in terms of irradiation and temperature. However, since the measurement was done in winter, there are only a few data points with suitable irradiation of more than 500 W/m<sup>2</sup>. Figure 4-16 shows the ratio of the measured voltage and the theoretically calculated voltage over the whole measurement interval from 09.11.2021 until 31.01.2022. Only voltage values with irradiation above 500 W/m<sup>2</sup> were considered.

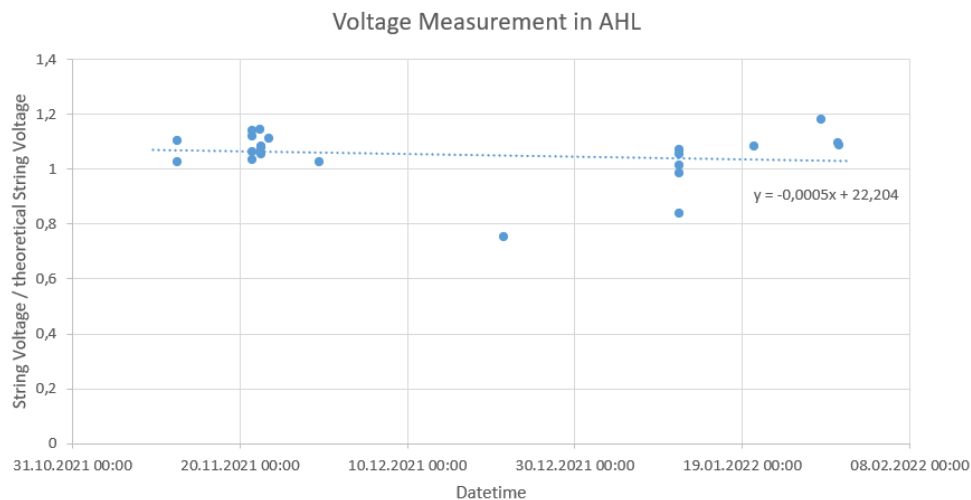


Figure 4-16 Voltage measurement in AHL  $V_{String}/V_{String,theo}$ .

It can be seen that no clear trend can be crystallized. The voltage does not seem to have improved over the test period. However, it is challenging to draw conclusions here. There is generally very little irradiation, which makes the calculation of the theoretical MPP voltage inaccurate. In addition, the values are only available every minute or, in the case of the sensor data, only every quarter of an hour. Furthermore, the measured module area is vast and includes several strings. Since the PID effect occurs preferably at the modules located at the end of the string, since the negative voltage with respect to ground is most significant there, the voltage increase to be expected is also not extremely large.

In order to determine a possible improvement of the MPP voltage due to the reversal of the PID effect, it is necessary to measure the voltage in smaller time intervals. In addition, it makes sense to keep the measuring range as small as possible and limit it to only a few individual modules. Furthermore, a time with higher irradiance should be waited for to obtain meaningful results.

### 4.3 Commercial Evaluation

In order to provide an estimate of whether the installation of the PVPB boxes is profitable and whether the costs will be recovered within the operating lifetime, the calculated yield gain from Chapter 4.1 is used ( $G_{Gain}$ ). Furthermore, a proportion of the DC nominal power of the area equipped with a PVPB box in relation to the total nominal power is needed ( $P_{Peak\ PID\ Area}$ ). Then, using this percentage value, the planned yield for this area ( $W_{Plan\ Yield\ PID\ Area\ 2021}$ ) was calculated based on the total planned yield in 2021 for the entire solar park ( $W_{Plan\ Yield\ 2021}$ ) as it can be seen in Formula 4.1.

$$W_{Plan\ Yield\ PID\ Area\ 2021} \left[ \frac{kWh}{a} \right] = W_{Plan\ Yield\ 2021} \left[ \frac{kWh}{a} \right] * P_{Peak\ PID\ Area} [\%] \quad (4.1)$$

The remuneration per kWh ( $R$ ) is composed of the fixed remuneration from the EEG and the management premium, which the direct marketer pays. A yield increase per year in Euros ( $G_{Yield\ Gain}$ ) can be calculated based on the additional calculated yield, the planned yield of 2021, and the remuneration rate as depicted in Formula 4.2.

$$G_{Yield\ Gain} \left[ \frac{€}{a} \right] = G_{Gain} [\%] * W_{Plan\ Yield\ PID\ Area\ 2021} \left[ \frac{kWh}{a} \right] * R \left[ \frac{€}{kWh} \right] \quad (4.2)$$

Based on the revenue per year and the installation costs, a break-even point ( $X_{Break\ Even}$ ) can be determined, which is a number of years. For the calculation of the break-even point, Formula 4.3 is used.

$$X_{Break\ Even} [a] = \frac{T_{Total\ Costs} [€]}{G_{Yield\ Gain} \left[ \frac{€}{a} \right]} \quad (4.3)$$

All required information and results are listed in Table 4-3.

Table 4-3 calculation of potential yield gain per year and break-even point

Park	Gain	Plan Yield 2021 [kWh]	Nominal Power of PID Area	Plan Yield PID Area 2021 [kWh]	Remuneration [€/kWh]	Yield Gain [€/a]	Break-Even after x Years [a]
EHEU	0.66%	4,826,219	24.11%	1,163,416	0.2883	2,213.72 €	4.5
FOR	-0.60%	3,736,023	10.36%	387,205	0.2151	-499.73 €	-1.4
HAI	-1.58%	3,329,776	5.52%	183,769	0.2883	-837.09 €	-3.2
RICH	2.49%	5,991,220	25.21%	1,510,302	0.2883	10,841.96 €	0.2
HAL	0.00%	17,985,441	5.83%	1,047,656	0.1635	0.00 €	0
FREI	-1.15%	7,940,576	12.96%	1,029,356	0.1103	-1,305.69 €	-2.0
EGG	1.31%	20,489,403	4.96%	1,015,289	0.1635	2,174.60 €	1.0
AHL1	0.82%	8,550,492	4.15%	355,051	0.2247	654.19 €	3.8
AHL2	0.00%	8,350,927	4.19%	350,259	0.2247	0.00 €	0
AHL3	1.98%	6,517,993	5.01%	326,543	0.1916	1,238.80 €	2.2
AHL4	3.30%	12,493,358	2.61%	326,029	0.1916	2,061.42 €	1.4
AHL5	0.07%	11,793,144	2.76%	325,417	0.1916	43.64 €	64.5
ROHR	2.80%	4,467,088	50.00%	2,233,544	0.2087	-13,050.69 €	0.0
ELS	-0.71%	19,466,040	5.89%	1,145,908	0.2247	-1,828.15 €	-1.8

It remains to say that partly the solar farms have negative returns.

The following is a forecast of expected future costs. For this purpose, the number of PVPB boxes required for each solar park is determined and multiplied by the known costs for the



PVPB. To determine the labor costs, the labor hours incurred to date are multiplied by the number of PVPB boxes needed for the complete equipment of the solar park. Travel costs for installation are only counted once since only one trip to and from each park is required to add the remaining PVPB boxes. For most parks, the calculation is straightforward because the previous costs can be easily transferred to the other inverter station and thus can be multiplied. However, for some parks, the configuration changes slightly when the park is fully equipped with PVPB boxes and therefore requires an adjustment. The deviating configuration is mentioned in the section of the respective solar park. The boxes' costs also include the additional material needed for installation. This includes the PVPB extenders, fuses, and auxiliary material like cables and cable plugs.

For the solar park FOR nine more PVPB boxes are needed, as there are a total of nine more inverter racks in the solar park. The total resulting costs are therefore 6,529.28 €.

There are a total of three central inverter stations in the solar park HAI. In each of them there are several inverter racks with several sub-units. The configuration varies between the stations. Five more boxes are needed for the park. The costs for this amount to a total of 8,907.05 €.

In the solar park RICH, three more PVPB boxes are due, as there are a total of three more inverter pairs that need to be supplied with a PVPB. Together with the labor costs, the total costs are 6,566.13 €.

The solar park HAL has to be equipped with another 17 PVPB boxes, because there are 17 more inverters. The costs for the boxes and the installation costs together amount to a total of 28,686.86 €.

The solar park FREI requires seven additional PVPB boxes, as there are seven other inverters here which can also be equipped with a PVPB. The costs for material and installation amount to a total of 13,154.44 €.

A total of 20 additional PVPB boxes can be installed in the solar park EGG. The solar park is relatively large and therefore has 20 more inverters that can be equipped with a PVPB. Thus, the costs for the material and the installation add up to 35,566.50 €.

AHL1 contains a total of six stations, each with four inverter racks, which in turn each consist of six inverter racks. The sixth station consists of five inverter racks. Two PVPB boxes are

required for each station. In the sixth station, however, a third PVPB box is required. The total cost is therefore 21,278.43 €.

In AHL2 there is a similar situation as in AHL1. The park also consists of six inverter stations, each with four racks of six inverter slots. Two PVPB boxes are required per station. Since one has already been installed, only eleven are required. The total costs are 20,351.80 €.

There are five inverter stations in AHL3, each with four subunits of inverters. In one station, one subunit has already been equipped with a PVPB for testing, with the remaining three subunits still missing. However, for the further equipment of the park with PVPB boxes, one box per station is sufficient. Therefore, five more PVPB boxes are needed. The station in which one subunit is already equipped with a PVPB will be equipped with a PVPB extender to connect the remaining subunits as well. The remaining stations receive their own PVPB box. This results in a total sum of material and labor costs of 11,133.16 €. The same as for AHL3 also applies to AHL4&5. However, there are a total of ten inverter stations here, of which one subunit in each of them has already been equipped with a PVPB box. The costs for AHL4 thus amount to 26,877.31 € and for AHL5 to 24,905.86 €.

The situation is more straightforward in the solar park ROHR, as there is only one additional central inverter station. This would be equipped analogously to inverter station one. The costs for this thus amount to 3,218.20 €.

The park ELS is again vast and consists of 18 inverter stations, of which all need to be equipped with a PVPB. One has already been equipped, so 17 more PVPB boxes are needed for complete equipment. The costs for this amount to 30.185,63 €.

In Table 4-4, all relevant costs for the complete equipment of the investigated solar parks are listed again.

## Results

Table 4-4 Future costs for the installation of further PVPB

Park	needed PVPB Boxes	Costs for PVPB boxes	Installation costs	Total costs
FOR	9	3,958.88 €	2,570.40 €	6,529.28 €
HAI	5	6,346.85 €	2,560.20 €	8,907.05 €
RICH	3	4,924.05 €	1,642.08 €	6,566.13 €
HAL	17	25,208.66 €	3,478.20 €	28,686.86 €
FREI	7	10,380.04 €	2,774.40 €	13,154.44 €
EGG	20	30,262.50 €	5,304.00 €	35,566.50 €
AHL1	12	17,718.63 €	3,559.80 €	21,278.43 €
AHL2	11	17,710.00 €	2,641.80 €	20,351.80 €
AHL3	4	6,680.40 €	4,452.76 €	11,133.16 €
AHL4	9	14,887.15 €	11,990.16 €	26,877.31 €
AHL5	9	14,887.15 €	10,018.71 €	24,905.86 €
ROHR	1	1,667.80 €	1,550.40 €	3,218.20 €
ELS	17	25,723.13 €	4,462.50 €	30,185.63 €

## 5. Discussion

In the following chapter, the study results are evaluated and critically examined. Possible sources of error in the evaluation and measurement are mentioned, and the topic of occupational safety is highlighted. Finally, an outlook for the future is given.

### 5.1 Evaluation of Results

Power measurements of the strings were carried out in five of the 14 solar parks investigated. It was noticed that some strings performed worse than they should have according to the performance guarantee. However, the deviations are not very large, and there is no clear sign of PID.

The results are all valid but mixed. It cannot be clearly stated that the PVPB box reversed any PID effect that may have occurred. Some solar parks have shown a positive development, which speaks for an increase in yield by the PVPB box, but some parks have also shown a negative development after installing the PVPB box. Many factors influence the determination of the yield increase after installation of the PVPB box, such as shading, measurement inaccuracies, and failures of individual components, which were not identified and calculated.

It is not possible that the PVPB boxes have reduced the yield of a solar park since there is no additional degradation effect brought to the plant. The calculated negative yield changes are based on other reasons and are not due to the PVPB boxes. Not considered failures in the reports of the technical operation managers or the generally very low irradiation in winter make an exact evaluation difficult.

### 5.2 Possible Errors

As previously stated, it is essential to note that outages and partial outages must be excluded from the PVPB box yield improvement analysis. However, it is possible that this did not happen for all outages in the evaluation, as some outages are challenging to detect and not reported in the incident reports of the technical operator. If, for example, only parts of an inverter fail and these are only a few or even individual strings, the yield of a central inverter is only minimally reduced since the rated power of the failed part is only a fraction of the total rated power. Therefore, in order to be able to exclude such failures from the calculation, these failures must be listed in the technical reports. However, this is not always the case, especially for minor failures, and can therefore additionally distort the result. Complete failures of the

central inverters, on the other hand, can be easily identified, even without using the technical reports. If an entire central inverter fails, it does not provide any yield, and this can be easily identified by zero values in the yield data used. Moreover, such more significant failures are also often indicated in the technical reports.

Another inaccuracy that can skew results is the energy measurement of the inverters themselves. The inverters will measure the voltage and current at one point in the inverter to determine the power. This is important not only for monitoring and supervision but also for the self-sustainability of the inverter. This is because the inverter is designed for a specific power, current, and voltage. If the defined limits are exceeded or undershot, the inverter must protect itself and switch off or reduce the load. The inverter must know how much power it is currently converting to do this. Since every measurement is subject to a certain tolerance and measurement inaccuracies, the calculated yield value of an inverter is not always 100% accurate. With regard to the exact design of the inverter, however, the manufacturers tend to keep a low profile and do not publish detailed documentation of their inverters. Hence it is difficult to make a statement about how significant the error in the energy measurement of the inverter is and how considerable its influence on the evaluation of the expected additional yield by the PVPB box is.

Another source of error could be the data basis itself. The used data is downloaded from the associated monitoring portals of the respective technical operator. The inverters are saved with their associated DC nominal power of the solar field. The specific yield of the inverter is calculated based on the nominal power and the measured energy values of the inverter. One source of error may be that the nominal power of the corresponding module field is stored incorrectly. This case is unlikely, but it can happen. For example, if a repowering of the modules was carried out, old modules are exchanged for new modules, and the DC nominal power changes minimally. In most cases, the resulting connected DC nominal power is minor since, according to the EEG, no nominal DC power may be added to solar parks that are remunerated according to the EEG.

While not a mistake, the following point should still be considered. If, for example, as already mentioned, a module repowering was carried out, old modules were exchanged for new modules. Thus new modules are in the plant, which are possibly not yet affected by PID.

However, the prevention of PID is also quite reasonable in this case. This prevents above-average unanticipated degradation in plant performance.

### 5.3 Influence of the Season

As mentioned earlier, the PVPB boxes in the solar parks were installed in the time range of September to November. Thus, their evaluation phase falls during the low-irradiation months of winter. This can have several disadvantages for the evaluation and assessment of the results. The sun is generally positioned lower on the horizon in winter, leading to more shading, either by the own row shading or by shading of surrounding trees or bushes, which do not cause any shading in summer. As a result, parts of the plant affected by shading may perform worse than they should have. This deterioration, if it occurs in the reference area, can lead to an artificial improvement of the result and thus certify a positive advantage for the PVPB boxes, although in reality, the advantage does not exist or exists only in a reduced form.

Furthermore, there is generally low irradiation in winter, which can also occur in summer, but happens much more frequently and for a longer time in winter. Due to the fact that the irradiation is low, the solar park also generates less yield. However, since the measurement accuracy of the inverters is limited, and the measured values are available with a maximum of one to two decimal places, this adds an inaccuracy to the evaluation. For example, if the inverter equipped with the PVPB box has a specific daily yield of 3.0 kWh/kWp and the reference area has one of 2.8 kWh/kWp, the ratio of both values is one of about 107 %. However, if the irradiation is now poor and the inverter with PVPB box has a specific daily yield of 0.5 kWh/kWp and the reference area one of 0.4 kWh/kWp, the ratio is 125 %. These outliers distort the trend and should not be taken into account. Therefore, it is recommended to use good irradiation periods for the evaluation to reduce the inaccuracies as far as possible.

### 5.4 Personal Safety Risk

Probably the most crucial point in the operation of electrical equipment is the safety of persons who may knowingly work near the electrical components or unknowingly come into their vicinity. Therefore, it is of utmost importance that the operation of PVPB boxes is clear to any electrician working in an area where the PVPB box is connected. This becomes very clear again when an accident happens. In order to better understand the consequences of such an accident and to be able to assess the risks, an imaginary accident is assumed in which a person has received an electric shock from the PVPB box.

The imaginary incident occurred at the solar park ELS. A subcontractor of the technical operator is on-site to replace the power unit fans on four inverters. Among them is the inverter, which is equipped with a PVPB box for testing. The inverter is disconnected from the power supply on the AC and DC sides to carry out the work. Subsequently, the absence of voltage on both sides is determined. After ensuring the absence of voltage, the work begins, and it is started to replace the fans. During the work on the inverter with the PVPB box, the technical employee comes with his hand against a cable lug and felt an electrical flow. The work is immediately stopped, and after a measurement, it is found that 260 V<sub>DC</sub> is present. The reason for this is the PVPB box. The subcontractor has no injuries but has felt the electrical flow.

Inverters are regularly serviced and opened for repairs. The maintenance and repairs can be carried out by different personnel. Therefore, it is of utmost importance that all persons working in the solar park be informed about the PVPB box and its function to avoid electrical accidents. The first and easiest step is to make the presence of the PVPB box visible using a sign in the inverter station and to make clear that the PVPB box must also be switched off in order to be able to work on the inverter without danger. A further step is to integrate the PVPB box into the safety briefing of the solar park, which must be read and signed by every employee before entering the solar park.

To identify the danger of the current flow caused by the PVPB box, the human body's electrical resistance must be determined first. However, this is not easy to do, and an assumption must be made. The human body's resistance can vary greatly and depends on external conditions, such as the moisture on the skin. If the skin is dehydrated, the human body's resistance can reach up to 100,000 ohms. If the skin is broken or moist, the resistance can drop to 1,000 ohms [40]. Assuming the worst case, the body resistance of the human is 1,000 ohms. The current that has passed through the body can then be calculated using Formula 4.1. It is assumed that the voltage measured after the incident was also present during the contact.

$$I_{body} = \frac{V_{DC}}{R_{body}} = \frac{260 V_{DC}}{1000 \Omega} = 0.26 A \quad (4.1)$$

The calculated body current is 260 mA. However, this cannot happen because the maximum output current of the PVPB box is 60 mA. Due to its design, the PVPB box tries to keep up the 60 mA, and if the leakage currents theoretically become so large that they exceed 60 mA at the set voltage, the voltage collapses. This phenomenon is called derating. Formula 4.2 is used

to calculate the voltage that is applied to the live part shortly after a human touches it with a body resistance of 1 kOhm.

$$V_{DC} = R_{body} * I_{body} = 1000 \Omega * 60 \text{ mA} = 60 V_{DC} \quad (4.2)$$

It can now be assumed that a voltage of 60 V<sub>DC</sub> was present during the touching and that a maximum current of 60 mA flowed. This corresponds to a power of 3.6 W.

Voltages in the DC range of up to 120V are considered safe because human resistance is high enough that no dangerous current flow can occur [41]. It can therefore be said that the electric shock caused by the PVPB box is not dangerous. However, secondary accidents could occur due to the shock and the sudden withdrawal of the hand. For example, if the person working is standing on a ladder and unexpectedly receives an electric shock, the person may become so frightened that she or he falls off the ladder and causes serious injury. The electrocution itself may have been harmless, but the subsequent fall from the ladder can result in serious injury. Regardless of the risk of expected electric shock of a PVPB box, current flow through the human body must always be prevented. For this reason, the PVPB box must be switched off during work on the inverter or in the module field so that no current flow can occur.

### 5.5 Risk Analysis

One danger of the whole evaluation is that the PVPB box did not cause the additionally calculated yields but only standard deviations in the measurements. This was tried to be prevented as far as possible by evaluating the technical monthly reports, the snow days, and the comparison with the previous year. However, it can never be completely ruled out that incorrect assumptions are made. Moreover, if the possible yield gain is now assumed to be caused by the PVPB box, this can lead to economically disadvantageous decisions. Because, for example, if the entire solar park is equipped with the PVPB boxes, which causes high costs for the solar park, and if these do not bring the targeted additional yield, these costs reduce the return of investment of the solar park and therefore reduces the profitability.

Another risk is that the PVPB boxes are installed incorrectly. After all, it is another electrical device installed in the plant where faults can occur. Here, elementary mistakes can happen, such as the cable lugs are not correctly mounted on the cables and come loose after some time. These defective live cables can cause a short circuit. Another mistake that can be made is not installing the inline fuses on the DC cables on the DC busbars in the inverters or installing them too far away from the busbar. Suppose a fault occurs between the DC busbar and the



inline fuse. In that case, a short circuit will occur, which can have catastrophic consequences, such as a fire, which in the worst case will destroy the entire inverter station, including the transformer. This causes immense costs.

### 5.6 Outlook & Recommendation

The PID effect has not yet been eradicated and is still present in the solar industry. This is still the case, although solar modules could be built PID-free. However, solar modules must be very cheap, as competition is fierce. The purchase decision in investment projects usually falls on the cheaper modules, favoring the expected investment return. While solar module manufacturers could build modules that are largely immune to the PID effect, this would increase material and production costs, resulting in a significant economic disadvantage in the highly competitive solar module manufacturing environment.

Since high negative voltages to ground cause the PID effect, the problem with the PID effect will continue to increase in the future as the general system voltage of solar parks rises from 1000V to 1500V and even up to 2000V. More and more manufacturers in the solar business design their cables, connectors, inverters, and modules to handle up to 1500V. According to many manufacturers introducing the components, the increase in system voltage from 1,000 to 1,500 volts brings many benefits. For example, the higher voltage combined with lower currents results in fewer line losses. In addition, smaller, and therefore less expensive, cable cross-sections can be used. Furthermore, high-voltage technology enables strings to be up to 50 percent longer, thus resulting in less material being used. Overall, 1,500-volt solar farms are characterized by lower system costs. They are thus becoming increasingly attractive for achieving low costs, and thus good economic efficiency as purchase prices for solar power continue to fall [42].

The degradation through the PID effect is now well known and is already being addressed by inverter manufacturers. The manufacturers now equip their inverters with an anti-PID function as standard or offer an optional solution after additional payment. For example, the Sungrow 110CX inverter is already delivered with an anti-PID function as standard [34]. For the SUN2000 inverters from Huawei, the optional anti-PID modules integrated into the inverter must be purchased [35]. The problem of the PID effect has thus reached at least the inverter manufacturers, who directly integrate anti-PID solutions in their products or make the integration optional and available at an extra cost.

Regarding the investigation made in this thesis, no clear statement can be made for the solar parks whether a potentially occurring PID effect could be reversed since the results are still too variable and imprecise. Therefore, it makes sense to let the analysis and evaluation continue and repeat the evaluation in months with higher yields, such as May. However, it can be said that the PVPB boxes do not worsen the yield of the parks but are technologically capable of reversing any PID effect that may have occurred in the module field and thus increasing the yield or bringing it back to the original level, even if this effect is often difficult to prove.

## 6. Summary

In the investigation that took place as part of this master's thesis, a total of 14 solar parks were equipped with a PVPB box, which applies a repair voltage to the connected module array at night. Here, a positive voltage with respect to the ground potential is connected to the negative pole of the strings or junction boxes connected to the inverter. By applying the repair voltage, the PID effect should be reversed, as ions migrate from the module frame or the glass of the solar module back into the semiconductor of the solar module.

The solar parks investigated are exclusively solar parks with central inverter stations. For the investigation, only one inverter was equipped with a PVPB box in order to be able to evaluate it in comparison to the reference area subsequently. To make the evaluation more meaningful, all failures listed in the technical reports of the operators were excluded from the evaluation. Likewise, snow days were determined manually and excluded from the evaluation. In order to identify a seasonal effect, the same period from the previous year without the installation of a PVPB box was used for comparison.

As part of the thesis, a measurement of the voltage at the AHL solar farm was also made to better understand the function of the PVPB and to detect a possible increase in MPP voltage. The function of the PVPB box could be demonstrated very well. A possible increase in the MPP voltage of the connected module array could not be proven. This is mainly due to poor irradiation and the associated inaccurate calculation of the theoretical target voltage.

The results are very different and show partly negative and partly positive results. In the case of the positive results, it should be noted that with the positive development of only about 1%, the break-even point of the costs is already reached after one to four years and thus justifies the investment.

The possible sources of error in data acquisition and analysis are many. The influence of the low irradiation caused by the winter is significant and makes a rational analysis difficult. In addition, there are inaccuracies in the energy measurement of the inverters. Failures not reported in the reports also make a good evaluation difficult.

Of enormous importance is also the safety of people working in the area of the PVPB box. In order to avoid electrical accidents, it is essential to point out the PVPB Box and, if necessary, to include it in the safety training. The electric shock of a PVPB box is not necessarily fatal but

can be dangerous if the work takes place at height and then an electric shock occurs. Subsequent injuries may result from the shock. For example, falling from the ladder or hitting a neighboring component. To prevent such accidents, warning signs indicating the function of the PVPB Box should be and have been attached to all inverters and junction boxes equipped with PVPB Boxes.

The mixed results cannot be used conclusively to determine whether the PVPBs have enabled a reversal of the PID effect and thus generated an additional yield. However, it should be noted that apart from the yield losses during the installation of the PVPB boxes, there can be no reduction in the performance of the solar parks due to the PVPB boxes. To demonstrate a possible increase in performance due to the PVPB boxes, the analysis and evaluation should be continued and conducted again in higher radiation months, such as May or June.

With regard to the introduction of the standard 'TS IEC 62804-1:2015-08' in 2015, modules can be labeled as PID-free, although they may experience up to 5% performance degradation due to PID. Prior to 2015, references to PID or PID-free guarantees were omitted or not mentioned. PID can affect older modules manufactured before 2015 and modules manufactured after 2015. Therefore, it is also interesting for large portfolios to examine their portfolio for the PID effect.

However, it is clear that degradation due to the PID effect is still a hot topic and can reduce solar farm performance by a few percent. In extreme cases, significantly more. Nevertheless, the problem will not disappear in the future and will probably get worse. Photovoltaic modules must remain cheap to be profitable. In addition, solar parks are increasingly being designed for a system voltage of 1500V in order to minimize material costs and losses. The increasing system voltage makes the problem with PID increasingly worse.

## VI. References

- [1] ipcc intergovernmental panel on climate change, *Climate Change 2021: The Physical Science Basis*. [Online]. Available: <https://www.ipcc.ch/report/ar6/wg1/#FullReport> (accessed: Sep. 28 2021).
- [2] B. Gates, *How to Avoid a Climate Disaster*: Random House LCC US, 2021.
- [3] Climate Action Tracker, *Climate Action Tracker: Germany - Policies & Action*. [Online]. Available: <https://climateactiontracker.org/countries/germany/policies-action/> (accessed: Sep. 28 2021).
- [4] A. Detrick, A. Kimber, and L. Mitchell, "Performance evaluation standards for photovoltaic modules and systems," in *Conference record of the Thirty-First IEEE Photovoltaic Specialists Conference - 2005: Coronado Springs Resort, Lake Buena Vista, FL, January 3 - 7, 2005*, Lake Buena Vista, FL, USA, 2005, pp. 1581–1586. [Online]. Available: [https://ieeexplore.ieee.org/abstract/document/1488447?casa\\_token=7vHkJUI0VkcAAAAA:\\_V6ZQ1RcVKbFQkSznOD\\_1a8Nv4KnefHff3sp5FOdYdq6U81TwpxCxxL0iIHMMhbntI9Z53fprVU](https://ieeexplore.ieee.org/abstract/document/1488447?casa_token=7vHkJUI0VkcAAAAA:_V6ZQ1RcVKbFQkSznOD_1a8Nv4KnefHff3sp5FOdYdq6U81TwpxCxxL0iIHMMhbntI9Z53fprVU)
- [5] W. Luo *et al.*, "Potential-induced degradation in photovoltaic modules: a critical review," *Energy Environ. Sci.*, vol. 10, no. 1, pp. 43–68, 2017, doi: 10.1039/C6EE02271E.
- [6] V. Quaschnig, *Regenerative Energiesysteme: Technologie - Berechnung - Klimaschutz*, 10th ed. München: Carl Hanser Verlag, 2019. [Online]. Available: <https://www.hanser-elibrary.com/doi/book/10.3139/9783446461147>
- [7] *Band gap Band diagram Valence and conduction bands Semiconductor Electronic band structure*. [Online]. Available: <https://www.pngwing.com/en/free-png-hhwwx> (accessed: Sep. 30 2021).
- [8] K. Mertens, *Photovoltaics: Fundamentals, technology, and practice*. Hoboken, NJ, Chichester: Wiley, 2019.
- [9] V. Quaschnig, *Understanding Solar Cells*. [Online]. Available: <https://www.volker-quaschnig.de/articles/pv-basics/index.php> (accessed: Sep. 30 2021).
- [10] K. Mertens, *Photovoltaik: Lehrbuch zu Grundlagen, Technologie und Praxis*, 5th ed. München: Carl Hanser Verlag, 2020. [Online]. Available: <https://www.hanser-elibrary.com/doi/book/10.3139/9783446465060>

- [11] K. Niazi, Y. Yang, S. V. Spataru, M. U. Mutarraf, and D. Sera, "Experimental Benchmarking of Partial Shading Effect on Thin-Film and Crystalline-Silicon Solar Photovoltaic Modules," 2019, doi: 10.4229/EUPVSEC20192019-4AV.1.6.
- [12] J. R. Arabach, *Scheme of the layers for a typical PV module*. [Online]. Available: [https://www.researchgate.net/figure/Scheme-of-the-layers-for-a-typical-PV-module-12\\_fig2\\_333385614](https://www.researchgate.net/figure/Scheme-of-the-layers-for-a-typical-PV-module-12_fig2_333385614) (accessed: Mar. 4 2022).
- [13] K. Hara, S. Jonai, and A. Masuda, *Potential-induced degradation in photovoltaic modules based on n-type single crystalline Si solar cells*. [Online]. Available: <https://www.sciencedirect.com/science/article/pii/S0927024815001981> (accessed: Jan. 6 2022).
- [14] S. M. Karazi, I. U. Ahad, and K. Y. Benyounis, *Laser Micromachining for Transparent Materials*. [Online]. Available: <https://www.sciencedirect.com/topics/chemistry/soda-lime-glass> (accessed: Jan. 6 2022).
- [15] B. L. Allsopp *et al.*, *Towards improved cover glasses for photovoltaic devices*. [Online]. Available: <https://onlinelibrary.wiley.com/doi/full/10.1002/pip.3334> (accessed: Jan. 6 2022).
- [16] N. EKREN, *Researches on Anti-reflection Coating (ARC) Methods Used in PV Systems*. [Online]. Available: <https://pdfs.semanticscholar.org/b62f/17f0b8cf6c1faad2dc1ad2dcc25e6aedde43.pdf> (accessed: Jan. 6 2022).
- [17] Volker Naumann, Dominik Lausch, Klemens Ilse, Otwin Breitenstein, and Christian Hagendorf, *PID-shunting: Understanding from nanoscale to module level*. [Online]. Available: [https://www.researchgate.net/publication/266030328\\_PID-shunting\\_Understanding\\_from\\_nanoscale\\_to\\_module\\_level](https://www.researchgate.net/publication/266030328_PID-shunting_Understanding_from_nanoscale_to_module_level) (accessed: Dec. 3 2021).
- [18] S. K. Gaddam, R. Pothu, and R. Boddula, "Advanced polymer encapsulates for photovoltaic devices – A review," *Journal of Materiomics*, vol. 7, no. 5, pp. 920–928, 2021, doi: 10.1016/j.jmat.2021.04.004.
- [19] A. Kamboj, "Importance of negative or positive grounding of the central inverter in Solar Power Plant," *LinkedIn*, 13 Feb., 2018. <https://www.linkedin.com/pulse/importance-negative-positive-grounding-central-inverter-anup-kamboj> (accessed: Mar. 4 2022).
- [20] M. Sieg, *PID-bedingte Leistungsverluste im Solarpark – schwarzes oder weißes Schaf?* [Online]. Available: <https://www.pv-magazine.de/2015/10/13/pid-bedingte-leistungsverluste-im-solarpark-schwarzes-oder-weies-schaf/> (accessed: Dec. 2 2021).

- [21] K. Misbrener, *Crank it up: High-voltage solar systems save contractors cash*. [Online]. Available: <https://www.solarpowerworldonline.com/2018/11/high-voltage-solar-systems-save-contractors-cash/> (accessed: Dec. 2 2021).
- [22] A. Nuñez-Jimenez and R. Bkayrat, *Utility scale 1,500 VDC PV power plant architecture evolution: advantages and challenges*. [Online]. Available: [https://www.researchgate.net/publication/324208915\\_Utility\\_scale\\_1500\\_VDC\\_PV\\_power\\_plant\\_architecture\\_evolution\\_advantages\\_and\\_challenges](https://www.researchgate.net/publication/324208915_Utility_scale_1500_VDC_PV_power_plant_architecture_evolution_advantages_and_challenges) (accessed: Dec. 3 2021).
- [23] IEC, *IEC TS 62804-1-1: Technical Specification*. [Online]. Available: [https://www.vde-verlag.de/iec-normen/preview-pdf/info\\_iects62804-1-1%7Bed1.0%7Den.pdf](https://www.vde-verlag.de/iec-normen/preview-pdf/info_iects62804-1-1%7Bed1.0%7Den.pdf) (accessed: Dec. 14 2021).
- [24] D. de Rooij, *Potential Induced Degradation (PID): how to reverse or prevent solar PID?* [Online]. Available: <https://sinovoltaics.com/technology/potential-induced-degradation-pid-how-to-reverse-prevent/> (accessed: Nov. 16 2021).
- [25] V. Naumann *et al.*, *Explanation of potential-induced degradation of the shunting type by Na decoration of stacking faults in Si solar cells*. [Online]. Available: <https://www.sciencedirect.com/science/article/pii/S0927024813003000> (accessed: Dec. 9 2021).
- [26] R. Hirschl, "Potenzialinduzierte Degradation - Wirtschaftliche und Wissenschaftliche Aspekte," 2015. [Online]. Available: [https://padcon.com/files/wikiPIDia/PID\\_Praesentationen\\_Vortraege/PID\\_Wirtschaftliche\\_und\\_wissenschaftliche\\_Aspekte.pdf](https://padcon.com/files/wikiPIDia/PID_Praesentationen_Vortraege/PID_Wirtschaftliche_und_wissenschaftliche_Aspekte.pdf)
- [27] W. Luo *et al.*, "Potential-induced degradation in photovoltaic modules: a critical review," *Energy Environ. Sci.*, vol. 10, no. 1, pp. 43–68, 2017, doi: 10.1039/C6EE02271E.
- [28] SMA, *Modultechnik: SMA Wechselrichter*. [Online]. Available: <https://docplayer.org/15351221-Sma-wechselrichter-bieten-fuer-jedes-modul-die-passende-loesung.html> (accessed: Dec. 9 2021).
- [29] M. Schutze *et al.*, *Laboratory study of potential induced degradation of silicon photovoltaic modules*. [Online]. Available: <https://ieeexplore.ieee.org/document/6186080> (accessed: Dec. 9 2021).
- [30] S. Pingel *et al.*, *Potential Induced Degradation of solar cells and panels*. [Online]. Available: [https://www.researchgate.net/publication/224187548\\_Potential\\_Induced\\_Degradation\\_of\\_solar\\_cells\\_and\\_panels](https://www.researchgate.net/publication/224187548_Potential_Induced_Degradation_of_solar_cells_and_panels) (accessed: Dec. 9 2021).

- [31] J. Carolus, W. de Ceuninck, and M. Daenen, *Irreversible damage at high levels of potential-induced degradation on photovoltaic modules: A test campaign*. [Online]. Available: <https://ieeexplore.ieee.org/document/7936275> (accessed: Mar. 8 2022).
- [32] M. Cotterell, "PID and functional earthing," *Solar Power Portal*, 26 Nov., 2013. [https://www.solarpowerportal.co.uk/blogs/pid\\_and\\_functional\\_earthing\\_2356](https://www.solarpowerportal.co.uk/blogs/pid_and_functional_earthing_2356) (accessed: Nov. 16 2021).
- [33] P. Tumino, *Causes and Solutions of the Potential Induced Degradation (PID) Effect in PV Modules*. [Online]. Available: <https://eepower.com/technical-articles/causes-and-solutions-of-the-potential-induced-degradation-effect-in-pv-modules/#> (accessed: Nov. 16 2021).
- [34] *product / SUNGROW*. [Online]. Available: <https://ger.sungrowpower.com/productDetail/745> (accessed: Nov. 12 2021).
- [35] *SUN2000-(50KTL, 60KTL, 65KTL)-MO Benutzerhandbuch- Huawei*. [Online]. Available: <https://support.huawei.com/enterprise/de/doc/EDOC1100081160> (accessed: Nov. 12 2021).
- [36] PADCON GmbH, *PID KILLER*. [Online]. Available: [https://www.padcon.com/en/PID\\_solution\\_for\\_PID\\_affected\\_modules.html?file=files/ALTE\\_PADCON/Padcon/Produkte/PID\\_KILLER/Float%20Controller%20CI%20Family/EN/Broschuere%20PID%20KILLER.pdf](https://www.padcon.com/en/PID_solution_for_PID_affected_modules.html?file=files/ALTE_PADCON/Padcon/Produkte/PID_KILLER/Float%20Controller%20CI%20Family/EN/Broschuere%20PID%20KILLER.pdf) (accessed: Jan. 8 2022).
- [37] D. Schenker, *Produkte - PV performance DE*. [Online]. Available: <https://www.pv-performance.com/produkte.html> (accessed: Jan. 9 2022).
- [38] Google LLC, *Google Earth Pro*, 2021. Accessed: Oct. 12 2021. [Online]. Available: <https://earth.google.com/web/>
- [39] *UNI-T Voltage Meter, Multimeter, Oscilloscope | UNI-T*. [Online]. Available: [https://www.uni-trend.com/meters/html/product/General\\_Meters/Digital\\_Multimeters/UT61%20161%20Series/UT161B.html](https://www.uni-trend.com/meters/html/product/General_Meters/Digital_Multimeters/UT61%20161%20Series/UT161B.html) (accessed: Feb. 8 2022).
- [40] U.S. Department of Health and Human Services, *Worker Deaths by Electrocution: A Summary of NIOSH Surveillance and Investigative Findings*. [Online]. Available: <https://www.cdc.gov/niosh/docs/98-131/pdfs/98-131.pdf> (accessed: Feb. 15 2022).
- [41] T. Mühlenbruch, *Gefahren der Elektrizität*. [Online]. Available: <https://www.sonntaler.net/dokumentation/wiss/elektrizitaet/grundlagen/gefahren/> (accessed: Jan. 30 2022).



- [42] Energie-experten, *1.500-Volt-PV-Technologie auch in Deutschland wirtschaftlich*. [Online]. Available: <https://www.energie-experten.org/news/1500-volt-pv-technologie-auch-in-deutschland-wirtschaftlich> (accessed: Feb. 15 2022).

## VII. Affidavit

„Mitigation of the potential induced degradation of photovoltaic modules and its impact on the performance of solar parks“

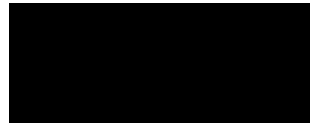
Written by: Jan Vollers

I hereby certify that I have independently written this Master's Thesis on the above-mentioned topic without any outside help and that I have used only the sources and aids indicated.

Passages taken verbatim or in spirit from the other works are identified with reference to the sources.

Date 11.03.2022

Signature:

A solid black rectangular box used to redact the signature of the author.

(Jan Vollers)

## VIII. Appendix

<b>Appendix</b>	<b>Description</b>
A2-7-1	Hanwha_Q_CELLS_Data_sheet_QPLUS_L-G4.2_340-350.pdf
A3-1-1	EHEU_module_datasheet_SF125x125.pdf
A3-1-2	EHEU_PVPM_measurment.XLS
A3-2-1	FOR_module_datasheet_CanadianSolar_CS6P_235P.PDF
A3-2-2	FOR_PVPM_measurement.XLS
A3-3-1	HAI_module_datasheet_SF125×125-72-M(L).pdf
A3-3-2	HAI_PVPM_measurement.XLS
A3-4-1	RICH_module_datasheet_REC JFJT Series Rev A.pdf
A3-4-2	RICH_module_datasheet_REC JM Series.pdf
A3-4-3	RICH_module_datasheet_REC_PE_series.pdf
A3-4-4	RICH_PVPM_measurment.XLS
A3-6-1	HAL_module_datasheet_BYD240_P6-30.pdf
A3-7-1	FREI_module_datasheet_CSI_CS6P235-255P.pdf
A3-7-2	FREI_PVPM_measurement.XLS
A3-8-1	EGG_module_datasheet_CSI_CS6P235-255P.pdf
A3-9-1	AHL_module_datasheet_CS6P-P.pdf
A3-9-2	AHL_module_datasheet_SunEarth_PV-Modul_235Wp_240Wp.pdf
A3-10-1	ROHR_module_datasheet_Sunowe_SF125×125-72-M(L)_EN.pdf
A3-11-1	ELS_module_datasheet_SF156_1565-60.pdf
A3-11-2	ELS_PVPM_measurement.XLS
A4-1-1	EHEU_PID_Evaluation.xlsx
A4-1-2	FOR_PID_Evaluation.xlsx
A4-1-3	HAI_PID_Evaluation.xlsx
A4-1-4	RICH_PID_Evaluation.xlsx
A4-1-6	HAL_PID_Evaluation.xlsx
A4-1-7	FREI_PID_Evaluation.xlsx
A4-1-8	EGG_PID_Evaluation.xlsx
A4-1-9a	AHL1_PID_Evaluation.xlsx
A4-1-9b	AHL2_PID_Evaluation.xlsx

## Appendix

---

A4-1-9c	AHL3_PID_Evaluation.xlsx
A4-1-9d	AHL4_PID_Evaluation.xlsx
A4-1-9e	AHL5_PID_Evaluation.xlsx
A4-1-10	ROHR_PID_Evaluation.xlsx
A4-1-11	ELS_PID_Evaluation.xlsx
A4-2-1	AHL_PID_Measurement_Evaluation.xlsx